Progress in Biophysics and Molecular Biology 137 (2018) 111–131

Contents lists available at ScienceDirect

Progress in Biophysics and Molecular Biology

journal homepage: www.elsevier.com/locate/pbiomolbio

Mathematical models of dorsal closure

A.C. Aristotelous [a, *], J.M. Crawford [b], G.S. Edwards [c], D.P. Kiehart [b, **], S. Venakides [d]

[a] Department of Mathematics, West Chester University, West Chester, PA, USA
[b] Department of Biology, Duke University, Durham, NC, USA
[c] Department of Physics, Duke University, Durham, NC, USA
[d] Department of Mathematics, Duke University, Durham, NC, USA

ARTICLE INFO

Article history:
Received 31 January 2018
Received in revised form
20 May 2018
Accepted 22 May 2018
Available online 29 May 2018

Keywords:
Computational
Actin
Myosin
Cell junctions
Cell sheet morphogenesis
Oscillation

ABSTRACT

Dorsal closure is a model cell sheet movement that occurs midway through *Drosophila* embryogenesis. A dorsal hole, filled with amnioserosa, closes through the dorsalward elongation of lateral epidermal cell sheets. Closure requires contributions from 5 distinct tissues and well over 140 genes (see Mortensen et al., 2018, reviewed in Kiehart et al., 2017 and Hayes and Solon, 2017). In spite of this biological complexity, the movements (kinematics) of closure are geometrically simple at tissue, and in certain cases, at cellular scales. This simplicity has made closure the target of a number of mathematical models that seek to explain and quantify the processes that underlie closure's kinematics. The first (purely kinematic) modeling approach recapitulated well the time-evolving geometry of closure even though the underlying physical principles were not known. Almost all subsequent models delve into the forces of closure (*i.e.* the dynamics of closure). Models assign elastic, contractile and viscous forces which impact tissue and/or cell mechanics. They write rate equations which relate the forces to one another and to other variables, including those which represent geometric, kinematic, and or signaling characteristics. The time evolution of the variables is obtained by computing the solution of the model's system of equations, with optimized model parameters. The basis of the equations range from the phenomenological to biophysical first principles. We review various models and present their contribution to our understanding of the molecular mechanisms and biophysics of closure. Models of closure will contribute to our understanding of similar movements that characterize vertebrate morphogenesis.

Contents

* Corresponding author.
** Corresponding author.
E-mail addresses: aaristotel@wcupa.edu (A.C. Aristotelous), dkiehart@duke.edu (D.P. Kiehart).

https://doi.org/10.1016/j.pbiomolbio.2018.05.009
0079-6107/

1. Introduction

Mathematical modeling is becoming an indispensable tool in the study of various processes of morphogenesis (Yu and Fernandez-Gonzalez, 2017; Sharpe, 2017), and in particular processes that involve the interaction between the components governing the function of a complex system. Models can be deterministic or stochastic, continuous or discrete, or finally a combination of all of the above (Murisic et al., 2015).

Ideally, a mathematical model identifies the salient features of a biological system and is based on the laws of physics and chemistry to describe and explain biological observations. When this is not possible, as is typically the case in biology, the modeler may seek the aid of phenomenological (empirical) laws, *i.e.* laws that arise from observation. A challenge then is for a deeper study to find scientific justification of such laws. In a related approach, alternative modeling approaches are introduced, competing with each other for the best recapitulation of biological (experimental) observation.

In all of these cases, the model consists of a system of mathematical relations, mostly equations, that involve the geometric, chemical and biophysical variables that participate in the model. The relations also include physical *parameters* such as moduli of diffusion or elasticity as well as other modeling parameters not explicitly correlated with physical quantities, that quantify phenomenological laws. For determining the values of various parameters that are not measurable in the lab, an optimization process is frequently implemented, in which the parameter values are chosen to optimize the agreement of the model outcome with the results of observation.

In the study of morphogenesis, what is mostly observed is the progress in time of biological form; the corresponding models are referred to as evolution models, where the term “evolution” is not used in its Darwinian sense. Solving an evolution model system of equations means using mathematical and computational tools in order to determine the state of the system (*i.e.* the values of the system variables) at any time past the known initial state of the system. For very simple models, it is possible, though rarely, to produce the solution in the form of a mathematical formula (for example, this occurs in Hutson et al., 2003). A benefit in this case is that the dependence of the solution on the parameter values is easily discernible.

Frequently, mathematical models are solved through simulation done via computer software, hence the term *computational models*. Through human effort, the modeling equations, typically differential equations, whose solutions are other functions, are discretized and approximated by a new system of a finite, though huge, number of algebraic equations whose solutions are numbers. The solution of the approximating algebraic system is reduced to simply performing the operations of arithmetic numerous times (*i.e.,* it could be billions) on a computer by using various computational algorithms. Each algorithm depends on how the modeling equations were discretized and has advantages and disadvantages. The choice of one over the others depends entirely on the type of equations at hand, the degree of desired accuracy and the cost of implementation. The results are presented in convenient table and graphical representations (*e.g.* plots or movies).

The focus of this review is on mathematical models, which geometrically are relatively simple, but biologically, the developmental process of the dorsal closure stage of embryogenesis in *Drosophila melanogaster* (Fig. 1) is relatively complex. Dorsal closure is a model for cell sheet morphogenesis and epithelial fusion with salient features and developmental mechanisms conserved across phylogeny and in wound healing processes (Gorfinkiel, 2016; Hayes and Solon, 2017; Kiehart et al., 2017; Harden, 2002; Hashimoto et al., 2015; Ray and Niswander, 2012; Heisenberg and Bellaïche, 2013; Heisenberg, 2009; Belacortu and Paricio, 2011; Razzell et al., 2014; Begnaud et al., 2016). Following the retraction of the germ-band, the dorsal surface of the embryo is filled with a sheet of large, flat, squamous epithelial cells, the amnioserosa, flanked by the smaller, elongated cells of the lateral epidermis formed by the retracted germ band. The term dorsal closure refers to the closure of this dorsal opening. Amnioserosa cells contract and produce force(s) for closure, ingress and eventually apoptose below the convergence of the lateral epidermal sheets that elongate dorsoventrally and meet and fuse at the dorsal midline. The leading edge cells of the advancing lateral epidermal fronts include actomyosin-rich cables that contribute a force to closure and the two advancing epidermal sheets converge at the canthi, the corners of the eye-shaped opening, where they are fused in a seamed, then a seamless epithelium in a process termed zipping (see Kiehart et al., 2017, Hayes and Solon, 2017 for review).

We analyzed existing computational models for dorsal closure to highlight the various techniques and approaches to model closure. Our goal is to help researchers in the field so they can build upon what has already been done. This should facilitate new efforts to develop novel computational models to describe the mechanisms that give rise to the various processes that contribute to dorsal closure. We seek to describe in sufficient detail the modeling approach used in some of the most well-known models and discuss their findings in order to provide insights for new or extended models.

This review has the following structure: Above we summarize closure and provide references for more detailed descriptions of the various cell movements and shape changes (the kinematics) and the forces (the dynamics) that drive such movements. In Section 2, we describe some of the biological processes/questions that have been raised and in Section 3, we identify some of the models in the published literature that were designed to address these questions. Then, in Section 4, we choose representative examples of those models and analyze their modeling approach, identifying some of their pros and cons and finally suggesting, whenever possible,

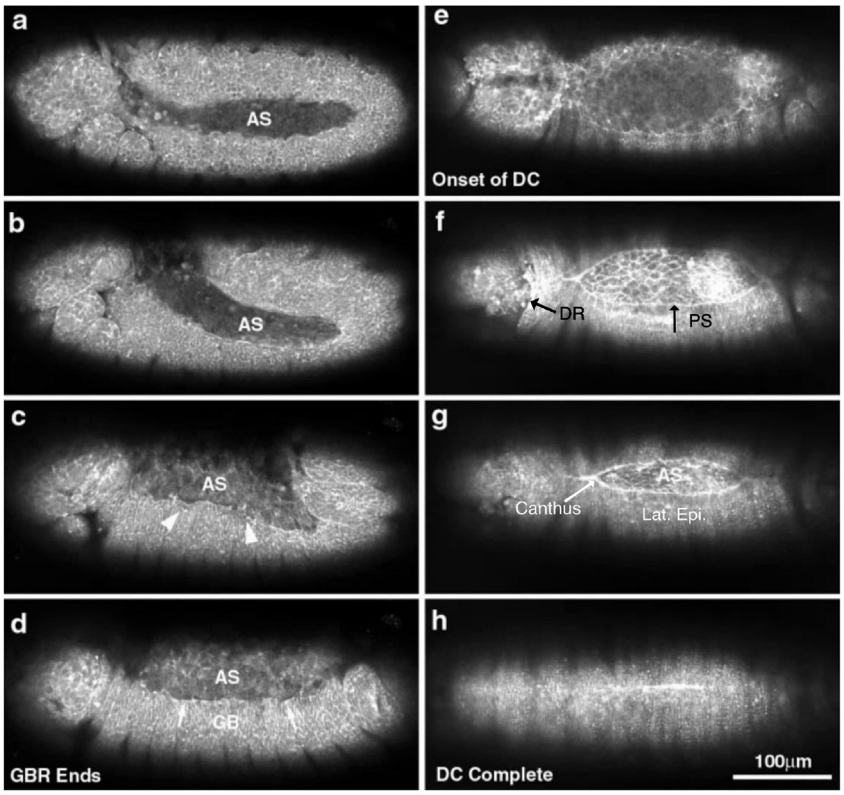

Fig. 1. Drosophila embryos undergoing germband retraction (a–d) or dorsal closure and head involution (e-h, anterior is to the left). The end of germband retraction (d) occurs about 9hrs and 20min after fertilization and following a 1–1.5hr gap, the process of dorsal closure requires approximately 2.5–3hrs to complete (at 25 C). Fluorescence is from the genetically encoded green fluorescent protein fused to the F-actin binding domain of Drosophila moesin (called sGMCA, see Kiehart et al., 2000) which labels F-actin. The amnioserosa (AS), the germband (GB), the actomyosin-rich cable or purse string (PS), the lateral epidermis (Lat. Epi) and the canthi are so designated. Arrowheads in c show the irregularly shaped leading edge of the lateral epidermis (see also Fig. 2). Arrows in d point to the accumulation of actin at the leading edge of the lateral epidermis. Black arrows in f point to the dorsal ridge (DR) indicating the progress of head involution and the dorsalward movement of the PS, respectively. Scale bar in h is 100 μm. Ultimately, the seam in h disappears as the formed dorsal epidermis becomes seamless (not shown). Reproduced and modified with permission (Kiehart et al., 2000, Fig. 1).

some ideas for their extension. We end with a discussion in Section 5.

In order to reach a wide audience, we have refrained from using mathematical equations in the main body of this review. The description in words will be adequate for the reader who has an extensive mathematical background and will not present an obstacle to the reader who does not. For all readership, we have included an appendix in which we outline the key equations that model basic phenomena, *e.g.,* the force equations for elasticity, contractility and viscosity for each of the models addressed.

2. Overview of observations and corresponding models

Morphogenesis during dorsal closure is a multi-scaled biological process composed of four distinct, but overlapping stages of closure. During the preclosure stage of germ band extension and retraction, epidermal cells intercalate, elongate and remodel their adherens junctions as the germ band retracts posteriorly, exposing the squamous amnioserosa layer that begins to oscillate or pulsate (Fig. 1 a–d, reviewed in Gorfinkiel, 2016; Lacy and Hutson, 2016; Kong et al., 2017). Following a 1–1.5 h gap period at the end of germ band retraction, the onset of dorsal closure stage begins with the dorsalward movement of the dorsal-most epidermal cells (DME), which remain tightly complexed with the peripheral amnioserosa (PAS) cells until the DME cells from opposing cell flanks meet at the dorsal midline (Fig. 1 e, Fig. 2 a–d). Over time, the initially scalloped leading edge of the DME cells accumulate F-actin and nonmuscle myosin II in a developing supracellular purse string that matures to form two smooth arcs of lateral epidermis tissue that join together at the canthi that form in the anterior and posterior ends of the dorsal opening (see Fig. 1 f–g, Fig. 2 b–d,f). The lateral epidermis tissue elongates toward the dorsal midline as a result of the elongation of first the DME cells, then of more lateral rows of epidermal cells (Young et al., 1993; Jacinto et al., 2002). At approximately the same time the canthi form, the leading edge of the DME cells become rich in filopodial and lamellipodial membrane projections (Jacinto et al., 2000, 2002; Eltsov et al., 2015). During the bulk of closure stage, zipping of the lateral epidermal sheets at the anterior and posterior canthi coordinates the constant decrease in the height and width of the dorsal opening and the constant radius of curvature of the advancing epidermal sheets – a key, emergent property of closure (Fig. 1 g, Fig. 2 c–d, f-g, Hutson et al., 2003; Jankovics and Brunner, 2006; Peralta et al., 2007). As the lateral epidermis advances, the amnioserosa cells continue to oscillate and ingress. During the endgame stage of closure, as the apposing flanks of lateral epidermis meet and fuse at the canthi, actin-rich filopodia play a key role in the proper alignment of developmentally patterned segments (Jacinto et al., 2000; Gates et al., 2007; Millard and Martin, 2008). Concomitantly, cell junctions between the DME and adjacent peripheral amnioserosa cells are remodeled and new cell junctions form between DME cells from apposing flanks of the lateral epidermis as they meet and fuse at the canthi through the interdigitation of lamellar sheets (Jacinto et al., 2000; Hutson et al., 2003; Wada et al., 2007; Lu et al., 2015; Eltsov et al., 2015). Following the remodeling of the junctions between the fusing lateral epidermal sheets, the seamed epithelium (Fig. 1 h,

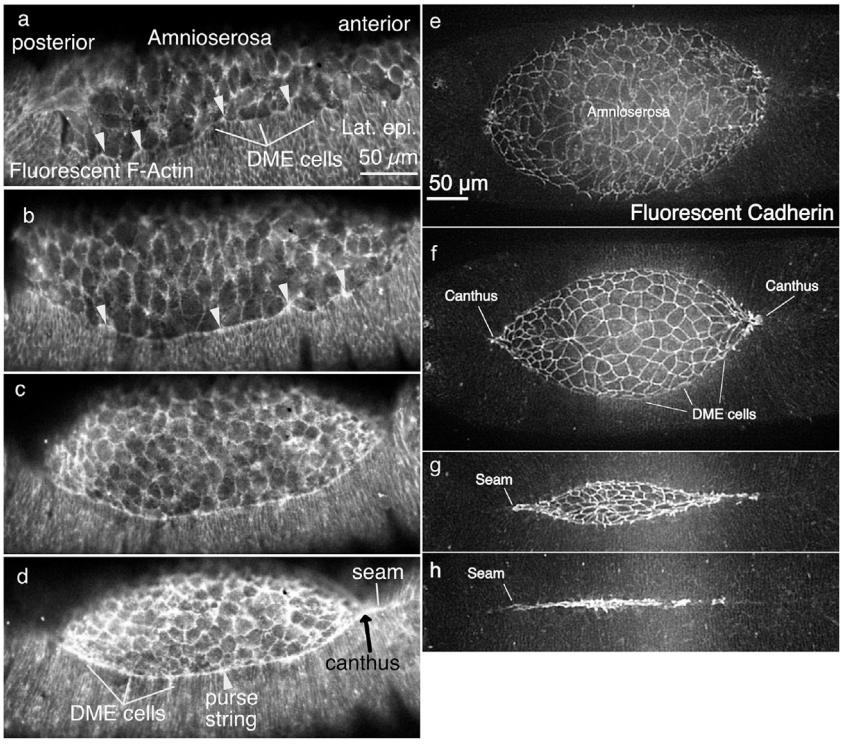

Fig. 2. High resolution view of transgenic Drosophila embryos expressing a fluorescent tag for F-actin (sGMCA; a-d) or E-cadherin (e–h) during dorsal closure. Posterior and anterior are the same in a-d and e-h and are labeled in a. Arrowheads in a, b and d indicate the accumulation of F-actin into the forming actomyosin rich cable or purse string (labeled in d) which forms near the leading edge of the dorsal most epidermal cells (DME, labeled in a and d) of the lateral epidermis (labeled in a) where it interfaces with the amnioserosa (labeled in a and e). Canthi mark the "corners" of the eye-shaped dorsal opening (labeled in d and f) and are the origin of the seam that marks the joining of two lateral epidermal sheets to form the dorsal epithelium. Ultimately, the seam disappears and the dorsal epithelium that results is seamless. Panel a–d reproduced with permission (Kiehart et al., 2017, Fig. 4). Panels e–h kindly provided by Regan Price Moore.

Fig. 2 h) becomes seamless.

Extensive experimental research has contributed to a better understanding of the biomechanics of dorsal closure. The forces that drive dorsal closure are contributed by the amnioserosa contractions and ingression coupled with apoptosis, the tension in the curved actomyosin rich purse strings, and zipping at the canthi that shortens the length of the purse strings while maintaining their curvature. Conversely, dorsal closure is opposed by elastic and/or contractile forces in the lateral epidermis. Recently, the requirement for a functional purse string as a force producer during closure has been questioned (Ducuing and Vincent, 2016; Pasakarnis et al., 2016), highlighting the need for further studies (Kiehart et al., 2017). Although the basic characteristics of the process of dorsal closure are well established and understood, extant questions remain about important mechanistic details governing the observed movements and how they impact the overall progress of closure. Mathematical models are used to shed some light on these mechanisms, on how the emergent properties of closure are generated and several studies have sought to account for how these forces drive closure (Hutson et al., 2003; Peralta et al., 2007; Layton et al., 2009; Solon et al., 2009; Almeida et al., 2011; Wang et al., 2012; Jayasinghe et al., 2013; Dierkes et al., 2014; Saias et al., 2015; Gorfinkiel, 2016; Hayes and Solon, 2017). Below, we highlight various contributions that used mathematical models as a tool in order to answer questions relevant to the forces that drive dorsal closure.

2.1. Amnioserosa oscillations and purse string function

Early, before the onset of dorsal closure, amnioserosa cells oscillate or pulsate (see Fig. 3 from Solon et al., 2009 also Sokolow et al., 2012; Wells et al., 2014; Gorfinkiel, 2016). These oscillations continue during dorsal closure and the apical cross sections of the amnioserosa cells have been quantified as a function of time. Cell and tissue level deformations result due to fluctutating levels of actively contracting actomyosin in both junctional belts and transient medioapical arrays (Blanchard et al., 2010; Gorfinkiel and Blanchard, 2011; Gorfinkiel et al., 2011; Martin and Goldstein, 2014; Gorfinkiel, 2016; Coravos et al., 2017).

The biophysical mechanism for and the biological significance of the oscillations is not fully understood. Various genetic manipulations can suppress oscillations without blocking closure. Nevertheless, they are a reproducible feature of closure that is being assessed experimentally. Moreover, their origin and mechanisms were the subject of study using mathematical models (Solon et al., 2009; Wang et al., 2012; Dierkes et al., 2014; Dureau et al., 2016). A common modeling approach is referred to by the molecular dynamics community as vertex models (Fletcher et al., 2013). In Solon et al. (2009) it is implied that the oscillation mechanisms might be an intrinsic property of the amnioserosa cells and the focus of the study shifted mostly to the description of the oscillations. In Wang et al. (2012) a hypothesis for what is actually generating the oscillations was tested by considering the existence of a signaling pathway that regulates the production of active myosin inside the amnioserosa cells. The work done in Dierkes et al. (2014) and Dureau et al. (2016) indicates that the mechanism for the oscillations might be attributable to non-linear elastic behavior coupled with the turnover of the actomyosin network of the amnioserosa cells without requiring an oscillating signal. While these oscillations are generally in anti-phase with their neighbors, occasionally patches of cells are observed to oscillate in unison (Wang et al., 2012; Solon et al., 2009; Blanchard et al., 2010; Gorfinkiel et al.,

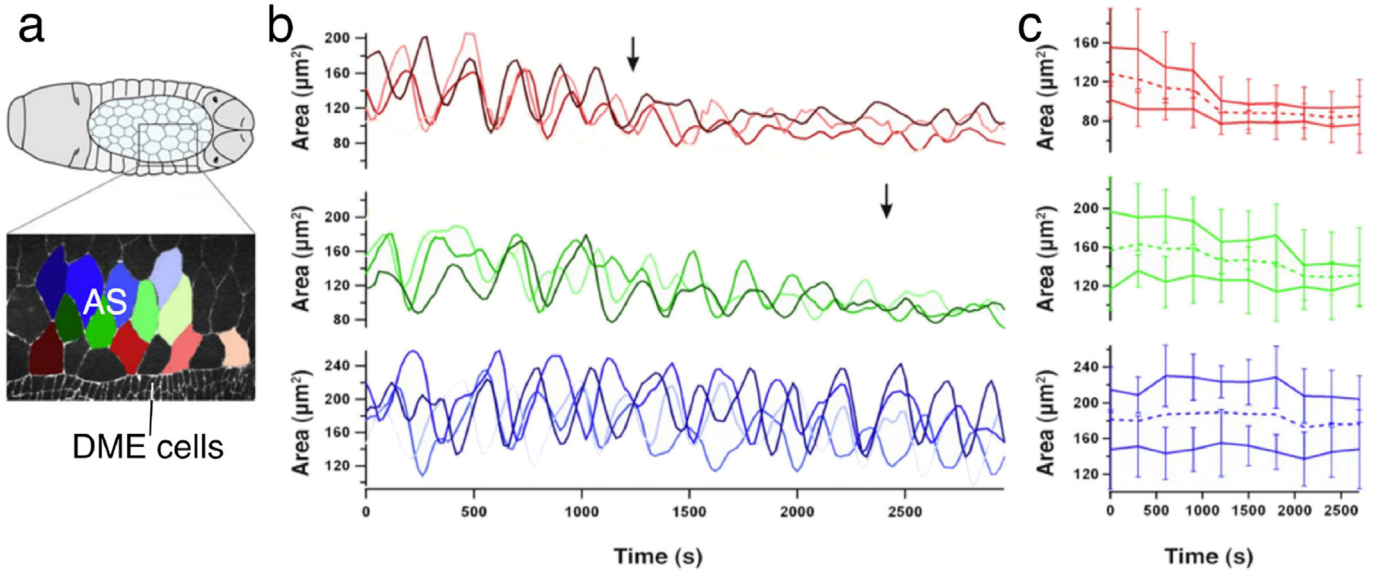

Fig. 3. Amnioserosal cell areas oscillate (or pulsate, from Solon et al., 2009). a. Upper panel: A schematic showing a dorsal view of an embryo after germband retraction but before the onset of dorsal closure (note, canthi have not yet formed). b. Lower panel: micrograph showing the interface between dorsal most epidermal (labeled DME) cells of the lateral epidermis and amnioserosal cells (labeled AS and corresponding to the boxed region in the upper panel). b. The oscillating areas of individual, colored cells in panel a are shown and are color coded to correspond to oscillations of the marginal cells of the amnioserosa (adjacent to the DME cells of the amnioserosa, upper, reddish traces), the second row of amnioserosa cells (middle, greenish traces) and the third row of amnioserosa cells (lower, bluish traces). Note, oscillations in amnioserosal cells persist longer if they are farther away from the DME cells. c. The average areas of the tracked cells for each row are plotted in panel c. The plots indicate that the marginal cells stop oscillating first, whilst the deepest, third row cells show the largest oscillations in cell area. Third row oscillations persist throughout the duration of the time studied. This further indicates that there is a progression of area loss from the marginal cells toward the middle of the amnioserosa. Reproduced with permission (Solon et al., 2009, Fig. 1, panels E–G).

2011).

What marks the onset of dorsal closure is the formation of a supracellular actomyosin cable and decreases in the amnioserosa cell volume that contribute to closure (Saias et al., 2015). The authors in Saias et al. (2015) developed a 3D biophysical model of how cell volume decrease of amnioserosa promotes closure progression. During the earlier stages of dorsal closure the amnioserosa contractions are slower than later in dorsal closure, once the canthi form and the onset of closure has begun (Gorfinkiel et al., 2009; Machado et al., 2015). A gradual decrease in their amplitude and period is accompanied by shrinkage in their respective areas (Blanchard et al., 2010). Following experimental work (Kiehart et al., 2000; Jacinto et al., 2002), mathematical models were developed incorporating the actomyosin cable as a purse string that helps the amnioserosa drive closure (Hutson et al., 2003; Layton et al., 2009). We note that in Layton et al. (2009) cell oscillations were not studied. In Solon et al. (2009) the idea of external and internal ratcheting and the sequential arrest of the amnioserosa cells was studied. This led Wang et al. (2012) to develop a model of cell oscillation and applied the idea of external and internal ratcheting (Gorfinkiel et al., 2009) to arrest the cell oscillations, which in their model were regulated by a signaling pathway that regulates myosin.

Following the arrest of the amnioserosa cells oscillations, the cell edges straighten and the closure speed increases noticeably as the concentration of actomyosin networks, on the apical side of the amnioserosa cells, progressively increases until it forms a global network on the apical surface (Blanchard et al., 2010). Several studies have analyzed the linear speed of closure and other markers characterizing dorsal closure (Hutson et al., 2003) and the governing forces due to the action of the amnioserosa, actomyosin cable and lateral epidermis (Peralta et al., 2007). Mathematical models were developed (Hutson et al., 2003; Layton et al., 2009) to recapitulate native closure and also scenarios with a mutant embryo and amnioserosa removal were explored with varying success. Almeida et al. (2011) used a fully continuum approach to model dorsal closure essentially ignoring cell oscillations.

2.2. Zipping

Another important component of dorsal closure is zipping, that is, a process near the canthi that is due to the interdigitation of epidermal filopodia and lamellipodia (Fig. 4, Jacinto et al., 2000, 2002; Eltsov et al., 2015), leading to fusion between the opposing leading edges (Peralta et al., 2008; Lu et al., 2015). An empirical law of zipping that expresses the speed of zipping in terms of the angles between the purse strings and the dorsal midline, was proposed in Hutson et al. (2003) and was used with success in Layton et al. (2009) (Fig. 6 d,e). In subsequent work (Almeida et al., 2011) zipping is modeled by the action of a force that is applied continuously to the purse string near the canthi, consistent with the experimental observations of Franke et al. (2005). Lu et al. (2015) presented a three-dimensional model for zipping in terms of the reaction dynamics of adhesion molecules that can be enhanced by amnioserosa forces.

3. Overview of models

The apical surface of the amnioserosa cells that fill the dorsal opening is where junctional belts and medioapical arrays of actomyosin are formed and contribute to the apical constriction of the dorsal opening. It is natural to assume a two-dimensional geometry, 2D, as a framework for constructing a mathematical model of dorsal closure. Nevertheless, especially at the beginning of closure, the amniosersa and the dorsal side of the embryo have real 3D character (Chen et al., 2014; Lu et al., 2016) and new models should take this three dimensionality into account. The majority of existing models indeed treat the amnioserosa as a 2D planar ellipsoidal or eye-shaped region (Hutson et al., 2003; Layton et al., 2009; Almeida et al., 2011; Solon et al., 2009; Wang et al., 2012; Dureau et al., 2016;

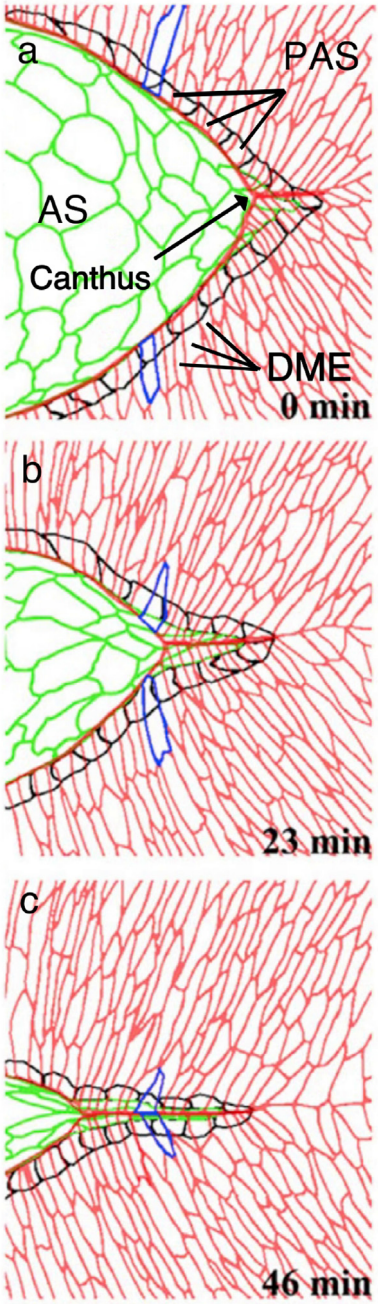

Fig. 4. Hand traced schematic of zipping at the posterior canthus. a. At the beginning of the time-lapsed movie these images were traced from, canthi had just formed. Peripheral amnioserosa (PAS) cells are traced in black and three adjacent PAS cells are labeled in a. All other amnioserosa (AS) cells are traced in green. Lateral epidermal cells are traced in red except for two dorsal most epidermal (DME) cells in each panel, which are traced in blue and can be followed from free leading edge (in a) to two cells away from the canthus (in b) to a position six cells into the seam (in c). Three adjacent DME cells are shown in a. Time is from the beginning of the time-lapsed video sequence and is shown in the lower left hand corner of each panel. Reproduced with permission (Lu et al., 2015, Fig. 1, panel F).

Dierkes et al., 2014). The domed curvature that characterizes the amnioserosa particularly early in closure (Fig. 5) is mostly ignored since the models attempt to keep the salient features of amnioserosa contraction and disregard secondary features that lead to complications and may not contribute to understanding.

There are models that represent cells as sets of nodes and edges (Solon et al., 2009; Wang et al., 2012; Dureau et al., 2016; Dierkes et al., 2014) and models where the cellular effects are homogenized to various degrees (Hutson et al., 2003; Layton et al., 2009; Almeida et al., 2011). For the first type of models, nodes and edges may come from image processing of real amnioserosa cells or they be can generated by Voronoi tessellation of idealized amnioserosa geometries or simply from hexagonal mesh representations of cells. Appropriate kinetic and dynamic equations incorporating biophysical, biochemical and biomechanical aspects of dorsal closure drive the evolution of those nodes and edges and the shape of the tissues that they form.

In a quest for answering specific questions regarding the global biomechanics of dorsal closure, observations and geometrical measurements were made on native, laser and genetically perturbed closure (Hutson et al., 2003; Layton et al., 2009). Such measurements led to the determination of the geometry as well as relative values for the forces that contribute to closure. The study in Hutson et al. (2003) contained the first model for native dorsal closure in the spirit described above. In Almeida et al. (2011) a fully continuum approach is employed by the use of partial differential equations to model dorsal closure.

Representing amnioserosa cells as polygons (called vertex modeling Fletcher et al. (2013)), allows models to capture phenomena at the level of a single cell or patch of cells as well as tissue wide phenomena. Since the amnioserosa is comprised of approximately 200 cells at the onset of closure, having an equation on each vertex and edge is within the capabilities of modern personal computers. Thus, this type of modeling is very popular.

Some features of dorsal closure might be represented by phenomenological/emperical laws, *i.e.,* quantitative relations that are observed experimentally, even though sufficient understanding of the underlying biological mechanisms are not present. An example is the kinematic law for zipping developed in Hutson et al. (2003). Modeling may also propose an underlying mechanism that has not been established experimentally in order to facilitate the explanation of an observed phenomenon that is not well understood. An example for this is the use of a signaling pathway for the regulation of the production of myosin and the emergence of amnioserosa cell oscillations during the early and slow phase of dorsal closure (Wang et al., 2012). Models are also used to compare alternative theories for explaining various phenomena. By the consideration of four alternatives in Dureau et al. (2016), nonlinear elasticity stood out as the best explanation for amnioserosa cell oscillations.

On the issue of cell oscillations, Solon et al. (2009) and Sokolow et al. (2012) examined how they progress and how they eventually die out. In subsequent work, Wang et al. (2012) developed a model to examine what generates the oscillations, based on a conjectured signaling pathway that activates myosin. In an alternative approach to Wang et al. (2012), Dierkes et al. (2014) and its recent extension by Lo et al. (2018), assume that nonlinear elastic behavior of the tissue coupled with the turnover of force producing molecules facilitates the onset of the oscillations. Nonlinear mechanics also emerges as the optimal alternative of the four models in Dureau et al. (2016).

4. A closer view of models

Next, we present in more detail the modeling approach and results of a collection of models which examine various mechanisms governing dorsal closure. We first present models that deal primarily with the mechanics of dorsal closure at tissue scale and subsequently we present models that deal with the phenomenon of cell oscillations.

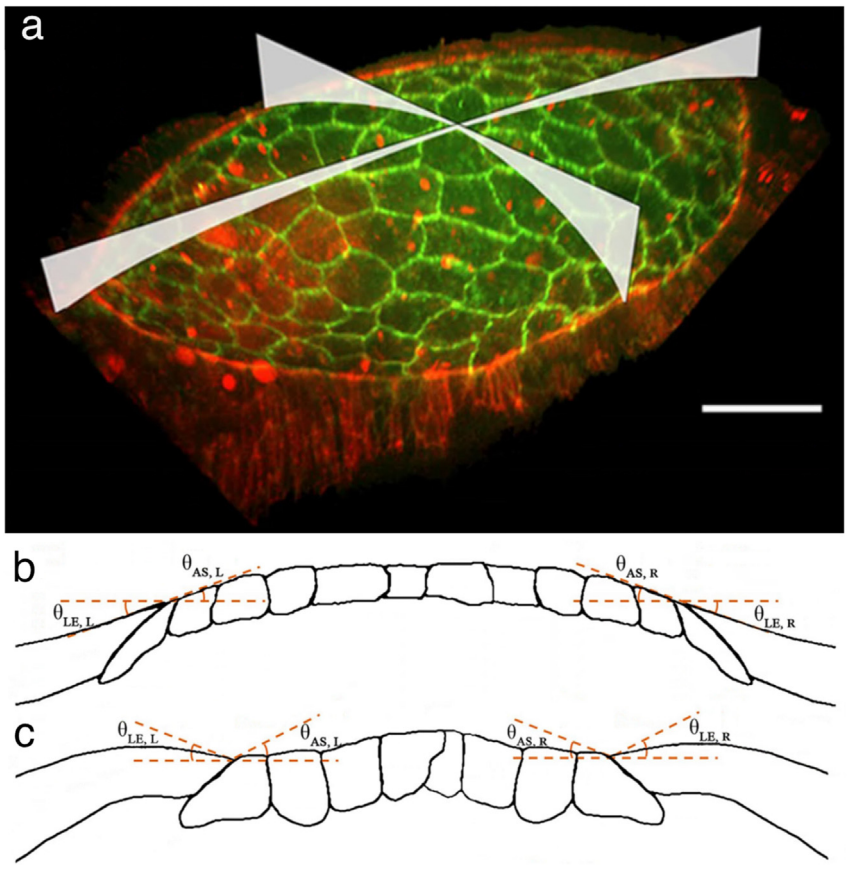

Fig. 5. Dorsal closure occurs in three dimensions. a. A domed amnioserosa characterizes *bona fide* closure, but models to date are largely two (and in one case, one) dimensional. Cell junctions in the amnioserosa are labeled with green fluorescent protein fused to *Drosophila* E-cadherin, cell margins in the lateral epidermis are outlined with a red fluorescent protein fused to the F-actin binding fragment of *Drosophila* moesin. Two orthogonal planes highlight the curvature of the domed amnioserosa in the anterior - posterior (AP) and dorsal-ventral (DV) axes. Scale bar is 50μm. b and c. Cell traces made from z-sections of the amnioserosa and flanking lateral epidermis early (b) and later (c) in closure. Angles are described in Lu et al. (2016). Future models will need to embrace the curvature of the tissues and their constituent cells. Reproduced with permission (Lu et al., 2016, Fig. 2 panels A,B and Fig. 3 panel C).

4.1. *Hutson et al., 2003; Peralta et al., 2007; Layton et al., 2009*

In Hutson et al. (2003), observations on native as well as laser and genetically perturbed dorsal closure are made, in conjunction with quantitative modeling. The equation for the balance of forces for closure is taken at the so-called symmetry points, the points of the two purse string arcs that project orthogonally to the midpoint of the dorsal midline (Fig. 6 a,b). The relative magnitude of forces is determined through initial recoil speeds after a laser cut has been applied (Fig. 6 c–g). At low Reynolds number, where inertial forces are negligible, Newton's Second Law reduces to the drag force being equal to the vector sum of three active forces: the ones exerted through the stresses of the amnioserosa and the lateral epidermis and the force due to the tension of the purse string. The latter force is proportional to the purse string tension times its curvature (equivalent to the reciprocal to the radius of the curvatures). Hutson et al. (2003) also developed a kinematic (without forces) model of closure, that simulated the geometry of the dorsal opening for wild type and mutant embryos, that disabled zipping at one or both canthi. These results predict a role for the β subunit of the integrin dimer (encoded by *myospheroid*) in the zipping process. This model of closure is the basis of subsequent models with forces (the dynamics) of closure *e.g.* Layton et al. (2009). The terms kinetic/dynamic arise from the Greek "$\kappa\iota'\nu\eta\sigma\iota\varsigma =$ motion", "$\delta\upsilon'\nu\alpha\mu\iota\varsigma =$ force".

The kinetic model is based on the phenomenological extension of a rate equation, including a rate constant for zipping, k_z. The equation relates mathematically the speed of zipping to the angles that the two purse string arcs make with the dorsal midline. The relation has the biophysically reasonable property that the speed of zipping increases as the angles become more acute. Nevertheless it idealized one zipping rate constant as applicable to both canthi. Further analysis subsequently established an asymmetry between the zipping-rate constants at the anterior and posterior canthi (Peralta et al., 2007). With two more assumptions, this relation turns into a differential equation that is solvable, indeed explicitly by formula. First, the two purse string arcs are assumed to be circular and congruent with each other, an assumption that is in fair agreement with the observed dorsal closure geometries. Second, the speed of closure at the symmetry points is assumed to be constant during closure, in very good agreement with observation during the bulk of closure. Given the shape of the dorsal opening once the canthi have formed, the formula that solves the differential equation produces the shape of the dorsal opening at any subsequent time, except during the very end of closure. The time evolution of the length, the width and the area of the dorsal opening calculated using the model are in good agreement with the corresponding experimental data from Hutson et al. (2003).

A natural step forward from the kinetic model is to pass to a dynamic model, dropping at the same time some of the observation-inspired assumptions of the kinetic model. This is pursued in Layton et al. (2009; see Fig. 6 above). The circular arc

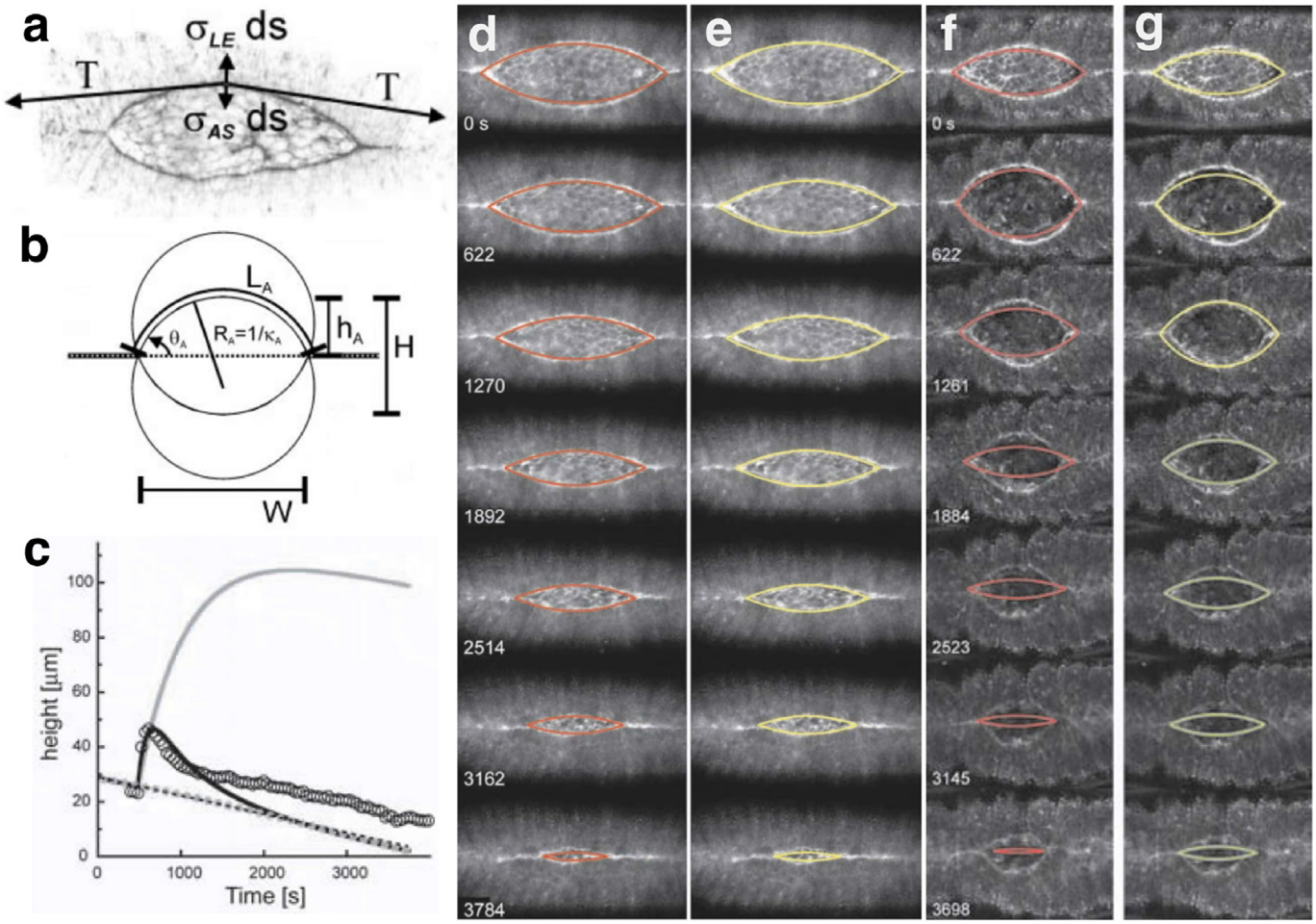

Fig. 6. The mathematical model of Layton et al. (2009) tracks wild type, native closure with precision, but fails to accurately track closure following surgical removal of the amnioserosa. a. The force balance diagram of Hutson et al. (2003) dictates the dynamics used by Layton et al. (2009) and includes forces from a purse string (the tension T), which is resolved in the direction of dorsal-ward movement as Tκ (not shown), from the lateral epidermis, σ_{LE} ds and from the amnioserosa, σ_{AS} ds. b. The circular arc geometry of Hutson et al. (2003) is consistent with an emergent property of closure in which zipping at the canthi maintains the strict relationship between the rate of change of the width of the dorsal opening (W) and the rate of change of its height (measured as the distance between advancing leading edges, H or the distance between the leading edge and the dorsal midline, h). The result is that the curvature of the leading edge changes only slightly during the course of closure. In Layton et al. (2009) adherence to circular arc geometry was relaxed. c. Plots of height vs. time illustrate the failure of Layton et al. (2009) to accurately predict the morphology of closure following surgical removal of the amnioserosa. Open circles are experimental data from an embryo in which a surgical cut removes the amnioserosa and AS. The model's prediction for a solely elastic tissue (gray line), for a solely contractile tissue (dashed gray line) and for a tissue that is both elastic and contractile (black line). d and e. The predicted evolution of leading edge morphology is super-imposed on micrographs of closure in a wild type, native (i.e., a non-surgically perturbed) embryo. The red line in d uses a linear force velocity relationship, the yellow line in e uses a hyperpolic force velocity relationship. f and g. The predicted evolution of leading edge morphology is super-imposed on micrographs of an embryo in which the amnioserosa was surgically removed. As in d and e, the red line in f uses a linear force velocity relationship whereas the yellow line in g uses a hyperbolic force velocity relationship. Panels a and b are reproduced with permission (Fig. 3 panel A is in Hutson et al., 2003). Panels c–g are reproduced with permission (Fig. 8 panel D and Fig. 9 panel B are in Layton et al., 2009).

assumption of the purse string of Hutson et al. is discarded. So is the assumption of the constancy of closing speed at the symmetry points. The empirical zipping law and the symmetry of the geometry with respect to the dorsal midline remain. The values of the zipping coefficients k_z are based on earlier experiments. For simplicity, every point on the purse string is constrained to move only perpendicularly to the dorsal midline, an assumption that does not vary substantially from the path of points on real purse strings tracked experimentally. The initial stresses that the amnioserosa and the lateral epidermis exert on the purse strings, as well as the initial tension of the purse strings, are taken to be constant along the purse string with values that are determined based on experimental data. In the absence of experimental data, the stress that the lateral epidermis subsequently exerts on the leading edge is taken to be constant throughout dorsal closure. A more detailed description of the lateral epidermis force is given in Almeida et al. (2011). Naturally an experimental study of the stresses in the lateral epidermis would provide valuable, additional information.

A key issue for the modeling is the stress that the amnioserosa exerts on the purse string. In this model, apposing points on the two purse strings are connected by an element that spans the amnioserosa to mechanically connect these two points. Inspired by muscle force laws (Keener and Sneyd, 1998, chapter on muscle), each element consists of an elastic sub-element in series with a contractile one. This work explores the mechanical aspects with comparison of the differences between having a linear or a hyperbolic force-velocity relation in the contractile element. Moreover, a general drag coefficient that is constant is used to describe resistance to movement throughout the various tissues that contribute to closure.

The force balance equation (A.7; see Appendix) applies in the model at every point of the purse string, giving the speed of the point in terms of the forces. In addition to this equation, the complete dynamic model of dorsal closure includes two evolution

partial differential equations (PDE) and two ordinary differential equations (ODE). The PDEs (A.5) and (A.6) model the evolution of the amnioserosa stress at the leading edge and the tension of the purse string respectively, using a muscle-type elasto-contractile law. The two ODEs (A.8) model the evolution of the position of the two canthi through the empirical law of Hutson et al. (2003). The five equations are coupled (they must be solved together) and constitute an evolution system.

The model contains seven parameters that are determined by optimization: elastic and contractile moduli for the amnioserosa and for the purse string, an isometric force coefficient for the muscle type contractile elements of the amnioserosa and for the purse string and finally a drag coefficient. The optimization uses experimental time-lapsed data from six wild type, native embryos, resulting in remarkably accurate recapitulation of native closure at large time-scale (the small time-scale oscillations are beyond the realm of the model). Note that the term native refers to embryos that have not been subjected to laser cuts or pharmacological perturbation (whether genetically wild-type or mutant).

The model, then is given the challenge of recapitulating the results of the five experimental protocols of Hutson et al. (2003) with perturbed embryos, four experiments with laser dissections (removal of the entire amnioserosa, disabling anterior zipping, disabling posterior zipping, disabling both) and one experiment with the *myospheroid* mutant that has defects in functional integrin cell adhesion receptor subunits. The recapitulations were qualitatively accurate and quantitative deviations, especially in tracking wild type native closure at the end of closure and in tracking leading edge movements following surgical removal of the amnioserosa, offer hints on the possible improvement of the model, especially as more accurate experimental descriptions of each of the forces becomes available. To date, the amnioserosa removal protocol has yet to be recapitulated successfully, potentially because the model does not adequately address the amniosersas contribution to zipping.

4.2. Almeida et al., 2011

In Almeida et al. (2011) a fully continuum approach is used to model dorsal closure, using partial differential equations. Both the lateral epidermis and the amnioserosa are modeled as homogeneous and isotropic elastic membranes (Fig. 7).

For the model a two-dimensional rectangular domain that contains in its interior the amnioserosa and a part of the lateral epidermis is used in three stages in each time step: (1) Based on previous work on wound healing (Almeida et al., 2009), the displacement of the lateral epidermis tissue at every point of the lateral epidermis domain is modeled by the use of a simplified membrane model which resulted in solving the Poisson partial differential equation in quasi steady state. That is, the lateral epidermis is modeled as an elastic thin membrane ignoring the short time scale vibrations by solving the equation in steady state at each discrete time step, as time progresses. The pulling of the amnioserosa and of the purse string on the lateral epidermis as well as a zipping force near the canthi are imposed through the application of appropriate mathematical conditions (flux boundary conditions applied to the displacement variable) on the interface of the lateral epidermis with the amnioserosa (the leading edge) (Fig. 7 a). In order to simulate the tendency of the lateral epidermis to pull/stretch the amnioserosa, reasonable mathematical conditions are imposed at the boundaries of the rectangular domain at its top and bottom (parallel to the dorsal midline). On the left and right boundaries, zero displacement is assumed. (2) The location of the leading edge is updated computationally. (3) Once the new location of the leading edge has been determined, the displacement values on the leading edge are used as a boundary condition in conjunction with the Laplace equation to determine the displacement values in the interior of the amnioserosa (Fig. 7 b). The zipping mechanism is described by the use of a zipping force represented as an integral on points of the leading edge. The underlying equations in the model are solved by using finite elements, a method of spatial discretization of PDE's suitable for non-rectangular domains and curved boundaries, in this case, the leading edge. In order to quantify the interactions between the lateral epidermis and the amnioserosa in the conditions imposed at the leading edge, four parameters (C_1, C_2, C_3, C_4) are introduced in the model. C_1 is associated with resistance to stretching of the lateral epidermis, C_2 quantifies the tension of the purse string, C_3 (eventually absorbed into C_2) quantifies the balance of the stresses of the lateral epidermis and the amnioserosa acting normally on the leading edge. Finally, C_4 quantifies the component of the force of zipping that acts on the leading edge near the canthi, in the direction that is normal to the dorsal midline. The horizontal component of the zipping force is assumed to be zero. The parameters are determined (calibration of the model) by optimizing the geometry of the simulated closure with respect to observed geometries of native, unperturbed dorsal closure. The optimization implements a genetic algorithm approach (an algorithm that imitates the process of natural selection). The model was calibrated, then tested with embryos where the zipping force is perturbed through the action of spastin, a microtubule severing protein which is experimentally known to inhibit zipping.

Like Layton et al. (2009), who applied their model to closure in physically and genetically perturbed embryos, Almeida et al. (2011) applied their model to genetically perturbed embryos. To evaluate the performance of the zipping mechanism of the model, ten unperturbed and ten spastin-perturbed embryos were simulated (Fig. 7 c). The model obtains the force coefficients C_1, C_2, C_4, the vertical zipping coefficient k_z defined in Hutson et al. (2003) and the vertical velocity of native closure. Model generated data were compared using the empirical zipping law of Hutson et al. (2003) and were found to be consistent with them. When Almeida et al. (2011) investigated a symmetric anterior/posterior setting where the two models are applicable, they found that their model was more sensitive at capturing the down-regulation due to spastin than Hutson et al. (2003). Given the use of just three parameters, the precision of the recapitulation of the leading edge geometry during dorsal closure is impressive. The success in capturing the dynamics and the spatial distribution of the leading edge, is in part due to the use of partial differential equations.

Favorable comparisons are made with Hutson et al. (2003) and with Layton et al. (2009). Certainly, the Layton et al. (2009) model, had less flexibility in recapitulating the full geometry of the leading edge, since it allowed movement only perpendicular to the dorsal midline. Nevertheless it was able to recapitulate the severely perturbed cases of disabling the zipping through ablation at any or both of the canthi, the case of the *myospheroid* mutant and with some degree of success, the ablating of the full amnioserosa. It would be interesting to see the performance of the Almeida et al. (2011) model in those tests. We conclude that the models developed in Almeida et al. (2011) and Layton et al. (2009) have a complementary role and could lead to the creation of an even more flexible model by combining features from both. However, neither model deals with poleward pull that subtly displaces each canthus towards its respective end, nor do they evaluate the contribution of individual amnioserosa or lateral epidermis cells.

4.3. Solon et al., 2009

The mathematical model in Solon et al. (2009) addresses the

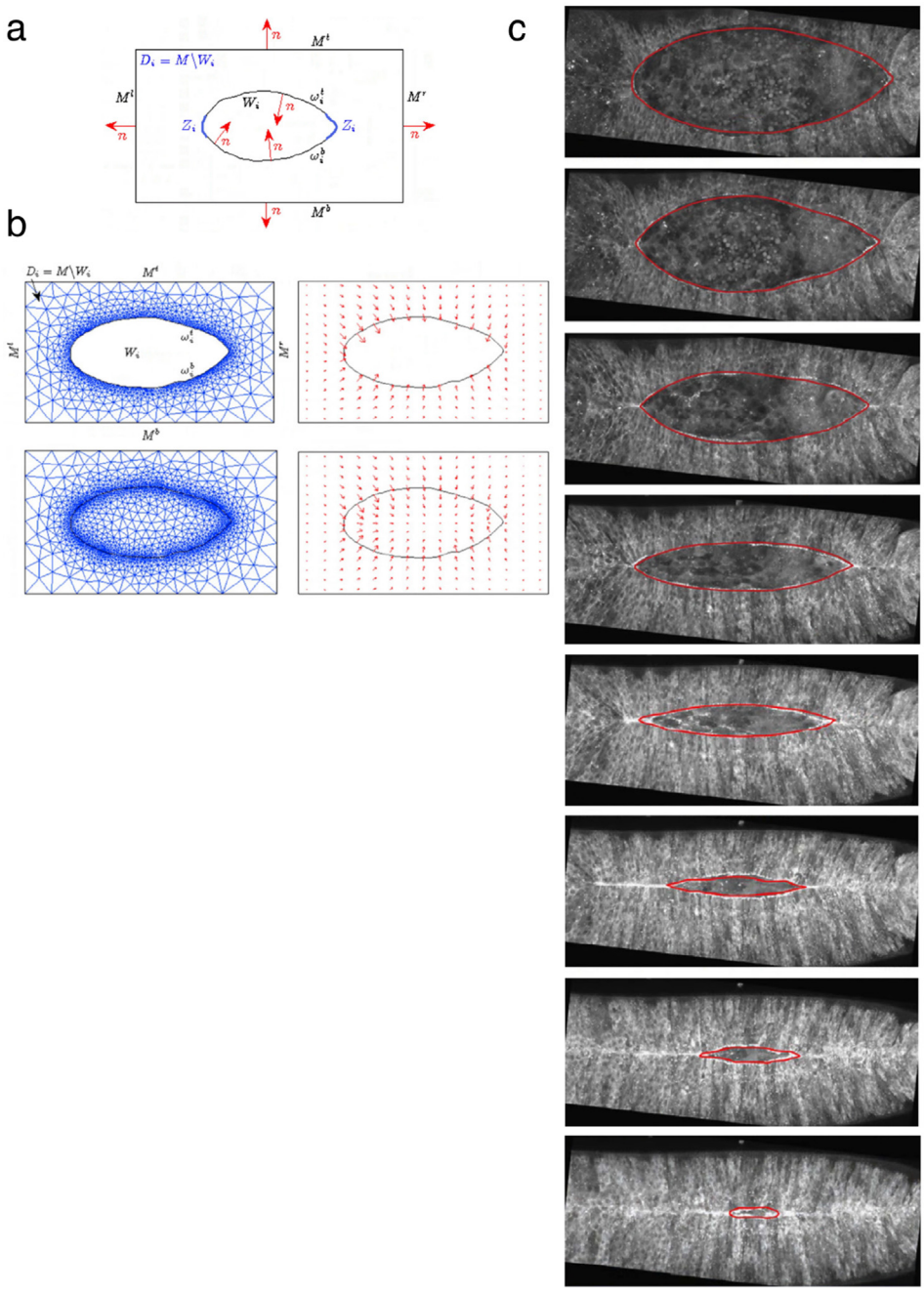

Fig. 7. The Almeida et al. (2011) model for dorsal closure. a. Panel a depicts the model's rectangular simulation domain D_i, with the irregular, ellipsoidal dorsal opening pictured and the two zipping domains at either end of the dorsal opening, Z_i, depicted in blue. Force vector fields operate on boundaries as shown. Details for other labels are provided by Almeida et al. (2011) Reproduced from Almeida et al. (2011), Fig. 3 b. Examples of computed solutions as shown in Fig. 4 of Almeida et al. (2011). c. Images of dorsal closure in an embryo expressing spastin, which inhibits zipping. The top four panels are from the left hand panels in Fig. 11 of Almeida et al. (2011), the next four are the three left hand panels and the bottom panel from Fig. 12 of Almeida et al. (2011). Red traces show that the model nicely tracks the evolution of closure in these genetically perturbed embryos. All figures are reproduced with permission (Almeida et al., 2011).

oscillations of the amnioserosa cells and hypothesizes that these oscillations are an intrinsic property of the amnioserosa cells. Using the vertex modeling approach discussed in Section 3, the model considers an ellipse-shaped two dimensional tissue and Voronoi tiling to depict the apical surface of the amnioserosa cells in the dorsal opening (Fig. 8). Each cell is represented as a polygon sharing its edges and vertices with neighboring cells (Fig. 8 b). The model focuses on the period prior to closure and early closure, before the formation of canthi and the onset of zipping, so zipping has been neglected. It is important to note that, oscillations occur during late germ band retraction (the embryonic stage before closure) and continue into closure so some features of the model apply even after canthus formation and the onset of zipping. The model includes the dorsalmost epidermal (DME) cells of the lateral epidermis. The action of the amnioserosa actomyosin network is represented by spokes connecting the cell center with each cell vertex. On each spoke and on the inner edge of each cell elastic springs are applied. Constant and uniform elastic properties are provided for every cell. For the production of sustained oscillations, the elastic constant of the leading edge springs had to be chosen

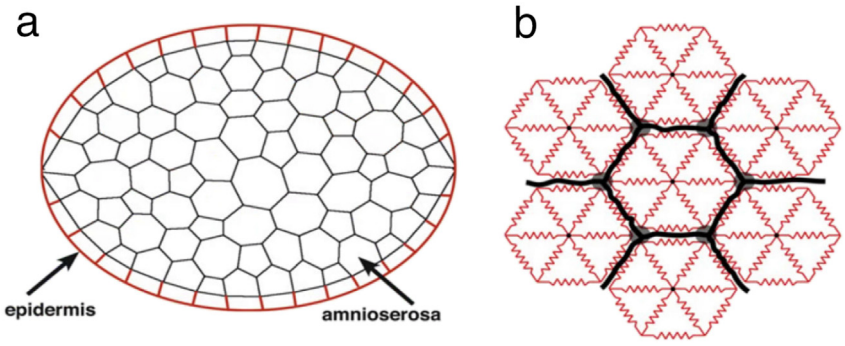

Fig. 8. The model of Solon et al. (2009) used to simulate oscillations in the amnioserosa during early dorsal closure stages. a. The geometry of the system includes 70 to 80 amnioserosa cells (outlined in black) surrounded by an elastic epidermis depicted in red. b. The distribution of elastic elements and the geometry of the model cell sheet is shown. Elastic springs shown in red connect neighboring vertices (gray dots) and each vertex with the center (black dot) of the hexagonal cell. Black lines show cell boundaries. Reproduced with permission (Solon et al., 2009, Fig. 7 panel A).

similar to the elastic constant of the amnioserosa cells. The velocity of each cell vertex, was taken proportional to the resultant force on the vertex, an assumption that accounts for the viscous, low Reynolds number environment described above, and again allows the omission of the acceleration from the equation of motion. It was found that oscillations are generated when a time-delayed contractile force with a saturation value is introduced, in addition to the standard elastic and drag forces. The contractile force depends on a mathematical formula (a Hill function. Hill, 1910, of order h, composed with tension as a function of time with a time delay τ), and on a critical cell-surface tension T_c, taken to be proportional to the cell area and presumably related to myosin-generated contractility. The balance of forces then produces oscillations that are sustained before there are formed purse string or actomyosin cable. This sigmoidal force may correlate with subsequent investigations of nonlinear mechanics and indeed such nonlinear mechanics have been proposed to account for the origin of oscillations (Dierkes et al., 2014; Dureau et al., 2016). Simulated stable oscillations occur during early dorsal closure, for a selection of the parameter values, *e.g.* Tension $= T_c$. Simulations reproduced qualitatively the cell-cell coupling, *e.g.,* the preference of a cell for pulsing in anti-phase with its immediate neighbors. Of course, any oscillations would be actively driven by actomyosin contractility due to ATP hydrolysis and a cell cannot oscillate passively in a low-Reynolds number (dramatically overdamped) environment. To initiate the onset of dorsal closure, the purse string/actomyosin cable are switched on in the simulation by additional springs positioned parallel to each boundary between an amnioserosa cell and the epidermal tissue. At the same time, a mechanism that boosts the tension T_c is introduced in order to compensate for the loss of tension effected by the gradual loss of tissue surface due to closure. The constancy of the amnioserosa tension in the process, modeled this way, is proposed as a result of observations following laser incisions. The tension-boosting mechanism acts first on the amnioserosa cells adjacent to the purse string, the so-called marginal cells Kiehart et al. (2017), subsequently extending its action to the inner cells, progressively in space and in time. It allows amnioserosa cell oscillations to die out progressively from the outer to the inner cells which is in general agreement with bonafide dorsal closure (Fernández et al., 2007; Solon et al., 2009; Blanchard et al., 2010; Sokolow et al., 2012). In the absence of this mechanism in the model, all amnioserosa cell oscillations would die out essentially at the same time. It is inferred that the formation of the purse string at the onset of dorsal closure sustains the lateral epidermis displacement and supports the amnioserosa-mediated force pulses to act like a ratchet (Solon et al., 2009). It is argued then that once formed, the purse string/actomyosin cable blocks the expansion of the of the pulsating ventral-most amnioserosa cells, in other words it blocks the retreat of the leading edge, sustaining the dorsalward displacement of the lateral epidermis, thereby functioning as a ratchet. A key attribute of this research is its molecular viewpoint; however, the ratchet proposal is controversial.

4.4. *Wang et al., 2012*

In the Wang et al. (2012) model the lateral epidermis and the zipping mechanism are omitted and the focus is on amnioserosa cell oscillations (Fig. 9). Building on Solon et al. (2009), the work of Wang et al. (2012) models the origin of the amnioserosa cell pulsing by considering the cyclic activation of myosin contractility. The work again uses vertex modeling with 81 amnoserosa cells, on a rhombus symmetric, hexagonal cell mesh. A signal is proposed to be the regulator of the production of myosin that is active (*i.e.* participates in closure) and the signal pathways are modeled phenomenologically due to lack of experimental data.

The actomyosin network inside each amnioserosa cell is depicted by spokes. On each spoke a linear algebraic equation is applied that describes the force on the spoke and incorporates in series contractility that is linearly dependent on myosin activity and a linear elastic component. Cell edges are modeled as linearly elastic springs. Assuming that junctional belts do not play a substantial role early in closure is reasonable, because many if not all cell margins are squiggly and probably are incapable of significant force transmission during early stages of closure. The motion of each cell vertex accommodates the viscous low Reynolds number environment in a way similar to Solon et al. (2009). The proposed signal pathway consists of the signal production equation that is coupled with myosin activity. Parameters for the model were chosen from the literature when available and the rest were estimated in order to produce results consistent with experimental observations. The model accurately sustained cell and whole tissue oscillations recapitulating experimental observations, with no net reduction of area. The cells were found to oscillate mostly in anti-phase with their neighbors in agreement with other works (Blanchard et al., 2010; David et al., 2010; Solon et al., 2009). It is argued that oscillation relies on the mechanical coupling among neighboring cells (Solon et al., 2009; Blanchard et al., 2010). This is indicated by the fact that parameter values at which a single cell oscillated did not necessarily produce sustained oscillation for the multiple cell tissue and led to the conclusion that the model recapitulates the hypothetical intercellular feedback mechanism proposed in Sokolow et al. (2012; see also Hunter et al., 2014). To mark the onset of dorsal closure, two ratcheting mechanisms were

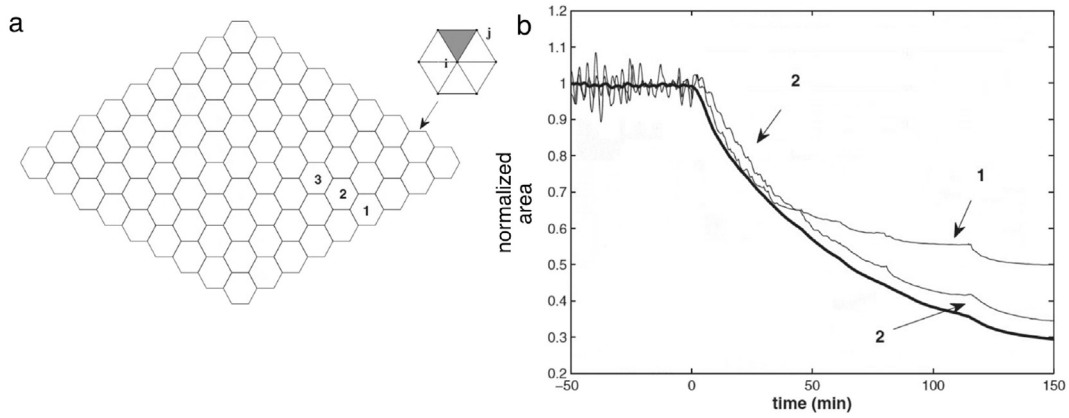

Fig. 9. The geometric basis of the model of Wang et al. (2012) is similar to that of Solon et al. (2009). a. It consists of a model amnioserosa consisting of 81 hexagonal cells - each cell has six edges and six spokes. The inset shows a cell with a shaded local triangle adjacent to a spoke, ij. Two such local triangles are used in their model to assess local area changes due to contraction of the spokes. b. Traces of normalized cell areas (thin traces for cells 1 and 2 in panel a) and normalized tissue area (thick trace) show the evolution of area loss with time. Reproduced with permission (Wang et al., 2012, panel a is from Fig. 1 and panel b is from Fig. 6).

modeled and were evaluated on their effectiveness in arresting the cell oscillations. First, as in Solon et al. (2009), a ratcheting mechanism representing the action of the actomyosin cable is implemented by activating at t = 0 two elastic bands along the outer boundary of the amnioserosa. Each is an elastic spring of modulus K and resting length of 125 micrometers, which is much shorter than the arc length of the interface between the amnioserosa and the lateral epidermis, extending between the canthi in the model. Thus, the actomyosin cable springs are under tension. The second ratcheting mechanism is being applied on each cell by reducing the resting length of each spoke and cell edge whenever the cell area reaches its minimum in each oscillatory cycle. Simulations showed that the internal ratcheting mechanism has a more important role than the actomyosin cable in arresting cell oscillations after the onset of dorsal closure. The bulk of closure dynamics are modeled phenomenologically, through shortening of the resting lengths. Later in closure, the myosin was observed to reach a steady-state level after oscillations are dampened by the ratcheting due to the phenomenological signal equation that dictates an equilibrium value of active cellular myosin. This myosin equilibrium concentration precludes, for example, the prediction of a sustained intensification of the actomyosin network later in closure. Similar to Solon et al. (2009), an attribute of this research is its focus on the regulation of actomyosin force production. Ultimately, the modeling work of this study propose a theory that awaits the advent of more detailed and definitive experimental data concerning the signaling pathways.

4.5. *Dierkes et al., 2014*

The question of cell oscillations was the topic also of the work performed in Dierkes et al. (2014). It is proposed that oscillations arise from the inherent coupling between the mechanical and biochemical degrees of freedom and do not rely on the presence of a chemical signaling network as suggested in Wang et al. (2012). In particular the proposed oscillatory mechanism is attributed to the nonlinearity of the elastic properties of the tissue coupled with the turnover of force producing molecules. Oscillation mechanisms for a single, one-dimensional contractile element and collective oscillations when such elements are coupled in series to form a chain are studied. In the (spatial) continuum limit of the oscillator chain, the diffusion of force producing molecules is modeled (Fig. 10). Firstly, the basic unit of the model is an element of length l, serving as a one-dimensional representation of a cell. The element is composed of three parallel-connected components: (1) a spatially homogeneous contractile element that represents a concentration c of force-producing molecules (myosins) appropriately interspersed with anti-polar actin filaments in the actomyosin network, (2) a nonlinear elastic spring element, and (3) a viscous damper. The model has two basic equations. The first equation describes the dynamics of the active myosin concentration c as it arises from two effects: (i) exchange of c with the reservoir, occurring with certain binding and unbinding rates, and (ii) conservation of mass, imposing that in the absence of turnover the product lc is constant. The second equation is a balance of forces, *i.e.,* Newtons Second Law at low Reynolds number. The drag force is the sum of the forces of the contractile and elastic elements. The contractile force is expressed in terms of c only. The elastic restoring force of the spring element is taken to depend nonlinearly on l. When coupled with the turnover equation, this system of two equations can recapitulate the oscillations for certain parameter regimes.

Three different scenarios are generated according to the choice of modeling parameters, partitioning the parameter space (phase plane) in three distinct regions (OP1, OP2, OP3). It was shown by doing bifurcation analysis and numerical simulation that, with the choice of parameters in the region labeled OP2 (Fig. 2b of Dierkes et al., 2014), the system $(c(t), l(t))$ undergoes sustained oscillations. In the parameter region OP1 the system tends to mechanical equilibrium, producing a steady, non oscillating force consistent with cell ingression and subsequent apoptosis (Sokolow et al., 2012). Finally in the region OP3 the model length collapses to zero in finite time which is non-physical. Critical values of parameters have been identified. The period of oscillations predicted by the mathematical model matched well experimental observations. A key attribute of the Dierkes et al. (2014) approach is that it is partially validated by comparing its theoretical oscillation frequency to the experimentally quantified oscillation frequency. More recently the Dierkes et al., 2014 approach has been extended to a more biologically realistic geometry (three dimensional molecular model) to unify oscillations and ingression in one nonlinear model (Lo et al., 2018). Secondly, the model considers a chain of units. The natural way to represent a collection of amnioserosa cells in this one-dimensional framework is by coupling the elements serially to form a chain. Collective oscillations were studied for the resulting chains, by adding a friction force that opposes movement of the boundaries between the elements relative to a fixed external substrate. The two ends of the chain are attached to a fixed elastic spring. The behavior of the system for zero friction and zero

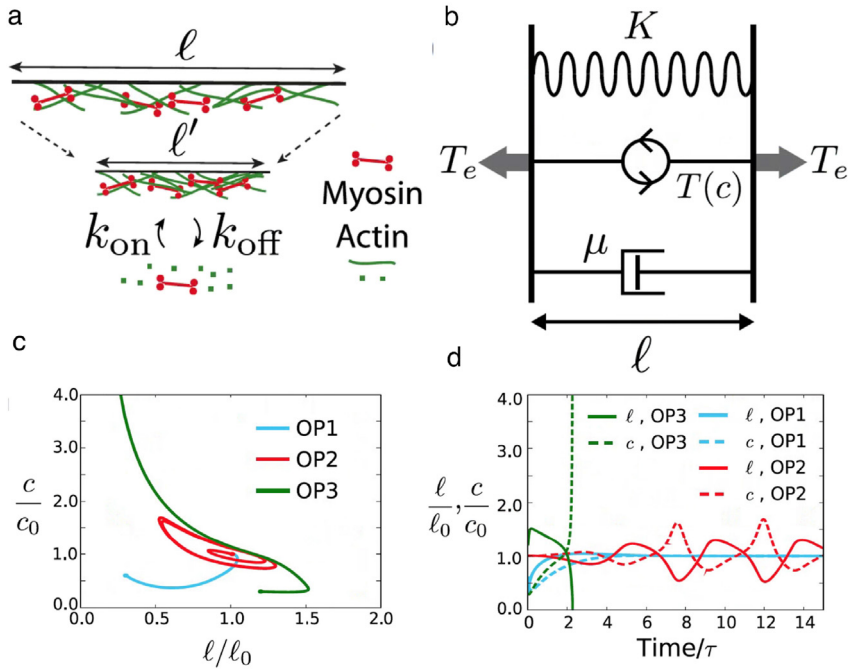

Fig. 10. The one-dimensional model of Dierkes et al. (2014). a. A schematic shows a cross section of the apical cortex of an epithelial cell with membrane (black line), actin filaments (green lines), actin monomer (green dots) and bipolar myosin filaments (red). Myosin filaments become concentrated when the cell contracts. They exchange with a reservoir with rates k_{on} and k_{off}. b. Depicts a schematic of a minimal model of a mechanochemical oscillator which includes a spring (top, squiggle) with spring constant K; a contractile element (middle, circle with arrows) that account for network contraction due to the hydrolysis of ATP by myosin and its motor activity associated with an actin filament; and a dashpot (bottom, with drag coefficient μ). The tension $T(c)$ produced by the contractile element is dependent on the concentration of active myosin. T_e is external tension opposing deformation of the contractile unit. c and d. Example of three trajectories of a contractile unit depicted in two different ways, phase plane (panel c) and as a function of time (panel d). The blue trajectory is stable (non oscillatory), the green trajectory "blows up" (unstable) and red indicates sustain oscillations. Reproduced with permission (Dierkes et al., 2014, Fig. 1a (panel a) and Fig. 2a, c and 2d (panels b, c and d, respectively)).

external force leads to uncoupling of the chain oscillators. On the other hand, for non zero external force it was determined, by doing a linear stability analysis and simulations, that the frictionless chain is in the class of globally coupled oscillators with a repulsive coupling. Further simulations showed that the chain of oscillators transitions from an uncoupled state with random phases for a small external coupling force to clustered states for a larger external force. The case of nonzero friction for a periodic chain of oscillators of constant length was considered. The linear stability analysis around the homogeneous state indicates that the nearest-neighbor anti-phase oscillations is the first to become unstable when the tension increases beyond a threshold value. Above this threshold, the units indeed oscillate in anti-phase in simulations. It was theorized that the difference in oscillation patterns with and without friction can be understood as follows. Without friction, the contraction of one unit results in a force acting equally on all other units, because the total force is conserved along the chain. With friction, contraction of one unit, initially only drives expansion of the nearest neighbors. Thirdly, the continuum limit of a chain in space is taken. To explain the observations, they studied the case where the concentration c diffuses between nearest neighbors by passing to the continuum limit of the chain (*i.e.* taking the number of basic units to approach infinity while keeping the chain length fixed). In the continuum limit the model is governed by a system of partial differential equations (PDE). By theoretically studying this PDE system and by performing simulations they determined that for certain choice of parameters there would be traveling wave solutions for c as observed in their experiments.

4.6. *Dureau et al., 2016*

Dureau et al. (2016) use a generic approach in modeling by considering mass-spring-damper vertex models, without taking into account the biologically realistic constraint of low Reynolds number. The properties of the amnioserosa and specifically the question of what generates the oscillations are re-examined. The study points out that the success of such models in 2D cellular systems is that they recapitulate two main physical features of live tissues, namely viscosity, which dissipates energy, and elasticity, which stores energy (Fig. 11). These properties are widely used to model biological systems, describing the dynamics of cells and tissues under various physical constraints. It is also pointed out that cells may change and/or adapt their mechanical characteristics over time, in response to external stimuli (*i.e.* stress softening or stiffening).

The study compares and contrasts four mass-spring-damper vertex models, each characterized by the effects that it includes. The goal is to identify the model that best recapitulates the cell oscillations in the amnioserosa. In all four models, each cell is represented as a polygon with a point mass m placed at each cell vertex. Each point mass connects to each of its neighbor point masses; it also connects to the barycenter (center of mass) of each of the cells it neighbors through spokes. In the basic model, each connection consists of an elastic element (linearly elastic model, LE). Adding a viscous element (damper) in parallel with each elastic element, defines the linear viscoelastic model (LVE). Introducing nonlinearity in the mechanical elements on each spoke in the LVE model, defines the third model (nonlinear viscoelastic NLVE). Finally, accounting for stress-independent myosin dynamics via the application of an external sinusoidal force onto each cell vertex of LVE, brings us to the fourth model (input-driven linear viscoelastic model, IDLVE) to account for myosin action. The sinusoidal force has common frequency and different phase shifts on each vertex and their values are obtained by optimization. All vertex masses m

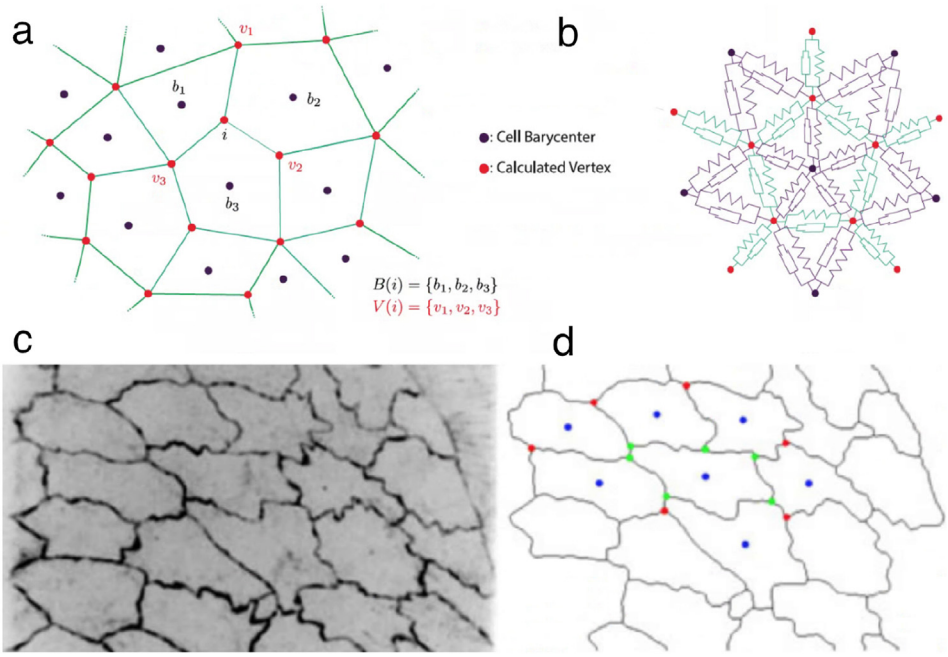

Fig. 11. a. The two-dimensional model geometry of Dureau et al. (2016). Red and purple dots indicate cell vertices and center of masses, respectively. Green lines indicate apical junctions between adjacent cells. b. Spring-dampers connect adjacent vertices (depicted in green, representing cortical visco-elasticity) and vertices and cell centers (depicted in purple and representing medioapical array visco-elasticity). The model tests the effectiveness of different kinds of visco-elastic linkages. c. A reverse contrast confocal image shows cell junctions, presumably labeled with fluorescent cadherin or one of its binding partners. d. A segmented image showing cell junctions (gray), cell centers purple, and multicellular junctions in red and green. Reproduced with permission (Dureau et al., 2016, Fig. 1, panels a and b, and Fig. 2, panels c and d).

are assumed to be equal. All elastic and viscous cell-edge elements are the same. This is also true for the spokes. The elastic and the viscous elements are characterized by constitutive laws, that is, the force produced by an element on its vertices. The force is given in terms of the element state (*e.g.* the extension of a spring) and in terms of parameters (*e.g.* the value of the spring constant) that quantify the property of the tissue that the element models. The state of each element varies as the cell geometry of the amnioserosa changes.

In order to represent the initial amnioserosa cell geometry, a confocal image of a patch of amnioserosa cells, showing their apical side, is segmented to a planar lattice displaying polygonal regions (the cells). As time increases, the cell geometry evolves, following the dynamical system of the modeling equations. These equations, formulated as a Lagrangian system, are essentially Newton's second law. The appropriate force magnitudes are obtained from the constitutive relations characterizing the elements (and the input force in IDLVE).

As pointed out above, each of the four models includes a number of parameters that quantify various tissue properties. These parameters (Dureau et al., 2016) are determined through an optimization process. More precisely, the system of the model differential equations (Euler-Lagrange equations obtained from the Lagrangian formulation of each model) is discretized and serves as a constraint to the optimization problem that minimizes the least squares cost function that penalizes the deviation of the mathematically derived data from the experimental and image processing data obtained during closure.

With the best fitting parameters determined for each model and after model validation using autocorrelation on the evolution of a selected vertex, the conclusion of the study is that the nonlinear visco-elastic model best fits the biological observations. It is interesting that this model (NLVE) does not take into account the action of myosin, yet outperforming the IDLVE which takes myosin into consideration. It would be interesting to consider as a new alternative an input-driven, nonlinear, viscoelastic model (IDNLVE). A concern about this modeling approach is it does not factor in the low Reynolds number condition common to other modeling efforts.

It is not clear how the conclusions of Dureau et al. (2016) are applicable to the dramatically overdamped environment of the embryo. The model selected by Dureau et al. (2016), the NLVEM non-linear visco-elastic model, has dissipation and does not have gain. This raises the question of how the action of myosin is represented in the model.

5. Discussion

The multidisciplinary research community investigating dorsal closure has had success in building mathematical models that quantify various aspects of dorsal closure and their mechanisms. Several different approaches have recapitulated the geometry of the dorsal opening as closure progresses (Hutson et al., 2003; Layton et al., 2009; Almeida et al., 2011). The amnioserosa is explicitly modeled in Layton et al. (2009), while the lateral epidermis is explicitly modeled in Almeida et al. (2011). Both models incorporated zipping, with Layton et al. (2009) utilizing the kinematic empirical law originally proposed in Hutson et al. (2003) and Almeida et al. (2011) using a zipping force in a continuum setting, with some improvement in the case of modeling one kind of mutant embryo. Additional research efforts have been focused on how amnioserosa cells can exhibit oscillations in their cross-sectional areas – a non-trivial research challenge given the low-Reynolds number (dramatically overdamped) environment of the embryo. Progress has been made with the use of vertex models that have provided three parallel interpretations for these oscillations as seen in Wang et al. (2012), Solon et al. (2009) and Dierkes et al. (2014). The origin of oscillations is attributed to signaling in Wang et al. (2012) and to nonlinearity in Dierkes et al. (2014), where the importance of nonlinearity was also identified in the subsequent work of Dureau et al. (2016). Subsequently it has been proposed that signaling of myosin binding to the actin network can regulate a switch from nonlinear oscillations to persistent

actomyosin forces that promote ingression (Lo et al., 2018).

Two decades of mathematical modeling and biophysical investigations have substantially advanced our understanding of the biological mechanisms responsible for the dynamics of dorsal closure. Systematic laser-perturbation experiments have demonstrated that not one process (amnioserosa forces, purse string forces, or zipping) is essential for dorsal closure, as the other process(es) can compensate (Kiehart et al., 2017; Hayes and Solon, 2017). A recent genetic pilot screen confirms these observations (Mortensen et al., 2018). Thus a system or systems of multiple processes provides a resilience and robustness that can overcome perturbations in cell structure and function that are present at the start of closure or develop as closure proceeds. Such systems promote the completion of dorsal closure in the face of remarkable odds.

Initially the modeling of dorsal closure was at the tissue length scale, but has now progressed to include molecular processes to address cellular dynamics, spanning multiple length scales. One example is the molecular models for cell oscillations and ingression, which are now factoring in how regulatory processes modulate actomyosin-based contractility. Initially the modeling of dorsal closure also idealized the process as two-dimensional, but has now progressed to fully three-dimensional models. One example is the three-dimensional, molecular and cellular model for zipping, which models the asymmetry in zipping at the anterior and posterior canthi as due to the molecular dynamics of interface remodeling in combination with differences in the tissue forces produced by the amnioserosa at each canthus (Lu et al., 2015). A second example is the three dimensional, time-dependent geometry of the dorsal opening, where analysis of the doming of the amnioserosa quantified its isotropic elasticity (Lu et al., 2016). A third example is the observation that the volume of an amnioserosa cell is not constant during dorsal closure, questioning the assumption that these cells would be isovolumetric and providing an extra force that may contribute to closure (Saias et al., 2015).

The success of the present models in providing precise mechanisms that explain observed phenomena of dorsal closure sets the stage for an ambitious modeling goal. This goal is to strengthen the connections between the understanding being gained through modeling and the extensive knowledge-base of dorsal-closure derived through developmental and biophysical studies of cell movements and their regulation. In other words, we see an opportunity to expand the modeling efforts to multiple scales, *i.e.,* from the tissue- and cellular-to the molecular-scale mechanisms that constitute the biomechanics of dorsal closure. For example, a more comprehensive model of cellular actomyosin structures may be achieved through novel models of interactions at the molecular level.

In such an overall effort, models and experimental work will have a more complementary role than they have today. Models will stimulate experiments that are designed to confirm or reject their validity. Additional experiments will cover new length scales to refine the modeling efforts. Ideally, tested models can be used to provide information on aspects that elude experimental approaches or are too costly to be performed. These models may be adaptive, in the sense that they can utilize updated information from experimental work as they run; an idea that was clearly expressed in Dureau et al. (2016). Globally, the modeling efforts will lead to further progress in sharpening our understanding of the underlying physical and chemical mechanisms that drive and regulate closure.

More generally, the models reviewed here face the same limitations as all models, not only the ones restricted to describing this biological process. Issues like multiple scales, *i.e.,* subprocesses evolving in different temporal and spatial scales and the various assumptions used to cope with these challenges, might limit the effectiveness of the models to make accurate and trustworthy predictions that could drive future experiments. An example is the lack of data/understanding at high resolution for intracellular processes that can affect the accurate description of the actomyosin network and its action within the cell. Increased resolution will have an impact in the construction of more biologically accurate models of dorsal closure.

Although significant strides in modeling dorsal closure have been clearly achieved, the modeling of dorsal closure maybe lagging behind the state of the art and modeling capabilities/techniques currently available and applied in other fields (like cancer research or biomedical engineering of tissues in general). These models, which often deal with multiple scales, use scalable algorithms which combine hybrid discrete-continuum, deterministic or stochastic, modeling approaches to approximate more explicitly the processes of interest, some directly in 3D. These models produce a multitude of data and simulations, that can help researchers explicitly visualize/understand better the phenomena (for examples see Cristini and Lowengrub, 2010; Jackson, 2012; Anderson et al., 2012; Gefen, 2013; Rejniak, 2016; Macklin et al., 2016; Ghaffarizadeh et al., 2018).

One can argue that the best model of biological complexity is one that answers the question at hand in the simplest manner possible. The relatively small number of cells and its small size make it possible to unleash the full potential of predictive modeling on dorsal closure. One can foresee using the existing computational power of modern day supercomputers and the advances in microscopy and imaging along with more detailed modeling of the intra-cellular processes in multiple temporal and spatial scales to construct a more comprehensive model that will explicitly simulate more parts of the entire embryo, thus limiting modeling assumptions and to a degree, uncertainty. This is a substantial challenge and it will require the expertise and collaboration from multiple fields.

We expect research progress in the mechanisms of dorsal closure to broadly impact our understanding of cell and tissue mechanics. Dorsal closure is a key model system for cell sheet morphogenesis and wound healing throughout phylogeny (Kiehart et al., 2017; Hayes and Solon, 2017). Essential features of cell sheet morphogenesis during closure, including characteristic cell shape changes regulated by conserved signaling cascades also specify morphogenesis during vertebrate neural tube closure, palate formation, heart closure, epiboly and wound healing (Ray and Niswander, 2012; Heisenberg and Bellaïche, 2013). During such movements, epidermal sheets migrate and/or change their overall shape to fuse and form a continuous epithelium. Moreover, several movements once thought to depend on the migration of single cells are now known to entail the migration of cell clusters or sheets. The migration of metastatic cancer cells and of neural crest cells provide excellent examples (Martin and Wood, 2002; Belacortu and Paricio, 2011; Heisenberg and Bellaïche, 2013; Pocha and Montell, 2014; Cai et al., 2016). In addition, understanding oscillations in amnioserosa cells shares common cause with understanding oscillations during mesoderm invagination. Thus, modeling efforts designed to provide insight into the mechanisms that drive and regulate various aspects of dorsal closure in fly, may well inform the basis of cell sheet movements and their regulation in vertebrate development and wound healing.

Acknowledgement

The research of ACA and SV were supported by NSF awards DMS 1720226 and DMS 1211638 respectively. The contribution of JMC, GSE and DPK was supported by NIH GM033830.

Appendix A. Supplementary data

Supplementary data related to this article can be found at https://doi.org/10.1016/j.pbiomolbio.2018.05.009.

Appendix A. Equations for Dorsal Closure

Each section below uses a sentence or short paragraph to clarify how the modeling team used equations to describe the underlying biology that contributes to dorsal closure. The identity of each variable and parameter is given in a table at the end of each section.

Appendix A.1. Hutson et al., 2003

The model assumes a purse string of two circular arcs that are symmetric to each other with respect to the dorsal midline, which is a reasonable approximation of the geometry of the dorsal opening during the bulk of closure. A force balance equation (Newton's second law at low-Reynold's number) is written at the symmetry points of the purse string, that project perpendicularly to the center of the dorsal midline and a phenomenological equation is proposed at the canthi, which is a modification of a rate equation by including the tanθ terms.

Force balance equation:

$$\sigma_{LE} - \sigma_{AS} - T\kappa = b\frac{dh}{dt} \quad \text{[Hutson } et\ al \text{ Eq 1]} \tag{A.1}$$

Phenomenological zipping law:

$$\frac{dW}{dt} = \frac{-k_z}{\tan\left(\frac{\theta_A}{2}\right) + \tan\left(\frac{\theta_B}{2}\right)} = \frac{-k_z W}{2H} \quad \text{[Hutson } et\ al \text{ Eq 2]} \tag{A.2}$$

Analytic solution of the model equations:

$$W(t) = W(0)\left[\frac{H(t)}{H(0)}\right]^{\frac{k_z}{2V}} = W(0)\left[1 - \frac{Vt}{H(0)}\right]^{\frac{k_z}{2V}} \quad \text{[Hutson } et\ al \text{ Eq 3]} \tag{A.3}$$

Table A.1
Parameters for Hutson et al. (2003).

Parameter	Units	Description
b	$\frac{nN*s}{\mu m}$	friction factor
k_z	$\frac{nm}{s}$	rate constant for zipping
κ	dimensionless	curvature of the purse string

Appendix A.2. Layton et al., 2009

The model traces the evolution of the purse string during closure. It makes the following basic simplifying assumptions:

1. All movements and forces are perpendicular to the dorsal midline.
2. The lateral epidermis stress at the leading edge, in the direction that is vertical to the dorsal midline is constant in space and in time.
3. The purse string is symmetric with respect to the dorsal midline.

These are reasonable approximations of the progression of leading edge cells, especially those cells near a symmetry point. Inspired by the Hill equation (Hill, 1938), the dynamic force-velocity law of the elasto-contractile elements of the model is given by:

$$\zeta\frac{dp}{dt} + \frac{\beta(p_0 - p)}{p + a} = v \quad \text{[Layton } et\ al \text{ Eq 9]} \tag{A.4}$$

The above law applied to an amnioserosa element, connecting two purse string points that are symmetric to each other with respect to the dorsal midline:

$$\zeta_{AS}\frac{\partial\sigma_{AS}}{\partial t} + \beta_{AS}\frac{\sigma_{AS} - \sigma_{AS,0}}{\sigma_{AS} + a_{AS,0}} = \frac{\partial h}{\partial t} \quad \text{[Layton } et\ al \text{ Eq 10]} \tag{A.5}$$

The same law applied to the purse string (the derivative of h is with respect to x):

$$\zeta_T\frac{\partial T}{\partial t} + \beta_T\frac{T - T_0}{T + a_T} = \frac{\partial\sqrt{1 + h'^2}}{\partial t} \quad \text{[Layton } et\ al \text{ Eq 12]} \tag{A.6}$$

Balance of forces at each point of the purse string, similar to the one in Hutson *et al*, with K_{PS} given Layton *et al* Eq 13):

$$\sigma_{LE} - \sigma_{AS} - TK_{PS} = b\frac{\partial h}{\partial t} \quad \text{[Layton } et\ al \text{ Eq 1]} \tag{A.7}$$

Hutson *et al* zipping law:

$$\frac{dx_{\text{ant}}}{dt} = \frac{k_z}{2\tan\theta_{\text{ant}}}, \quad \frac{dx_{\text{post}}}{dt} = \frac{k_z}{2\tan\theta_{\text{post}}} \quad \text{[Layton } et\ al \text{ Eqs 19 , 20]} \tag{A.8}$$

Table A.3
Parameters for Layton et al. (2009).

Parameter	Units	Description
p_0		isometric force
ζ_{AS}	$\frac{\mu m}{\sigma}$	elastic coefficient
ζ_T	$\frac{1}{\sigma*\mu m}$	elastic coefficient

Table A.2
Variables for Hutson et al. (2003).

Variable	Description
σ_{AS}	force per unit length of the amnioserosa
σ_{LE}	force per unit length of the lateral epidermis
T	tension of the purse string
κ	curvature of the purse string
h	distance from the dorsal midline to the leading edge along the symmetry axis
W	width of the amnioserosa
h	distance from the dorsal midline to the leading edge along the symmetry axis
$\theta_{A/B}$	angles at the canthi
H	distance from the upper and lower leading edge along the symmetry axis
V	rate of closure

Table A.3 (*continued*)

Parameter	Units	Description
β_{AS}	$\frac{\mu m}{s}$	contractile coefficient
β_T	$\frac{1}{s}$	contractile coefficient
$\sigma_{AS,0}$	σ	isometric forces per unit length
T_0	$\frac{\sigma}{\mu m}$	isometric forces per unit length
a_{AS}	$\sigma\mu m$	dissipation constant
a_T	σm	dissipation constant
b	$\frac{\sigma * s}{\mu m}$	viscous drag coefficient
k_z	$\frac{\mu m}{s}$	zipping constant

Table A.4
Variables for Layton et al. (2009).

Variable	Description
v	contractile speed
p	external load
h	distance of purse string point from the dorsal midline
σ_{AS}	amnioserosa stress at the leading edge vertically to the dorsal midline
T	tension of the purse string
$x_{\text{ant}}, x_{\text{post}}$	position of the anterior and posterior canthi
θant, θpost	angle the purse string makes with the dorsal midline

Appendix A.3. Almeida et al. (2011)

The Laplace partial differential equation (first equation in A.9) describes the elastic behavior of the lateral epidermis surrounding the amnioserosa. The lateral epidermis and the amnioserosa are contained within a rectangular domain. The model is a simplification of an elastic shell model called membrane model. The resulting equation is essentially the Laplace equation. This model, as described by the authors, "is mechanically questionable" but its relative simplicity allowed for more flexibility in its implementation and yielded clear predictions. The use of a partial differential equation allows the modeling of less-symmetric geometries, *i.e.*, more irregularly shaped dorsal openings relative to the model of Hutson et al. (2003). The remaining equations in (A.9) representing non-homogeneous Neumann boundary conditions that describe reasonable conditions on the sides of the rectangle (second and third equations) and conditions that model the action of the amnioserosa and zipping along the leading edge (equations four, five and six). The last two equations prescribe conditions for zipping in the part of the leading edge close to the canthi. Finally, the fourth equation models the action of the amnioserosa and is applied on the part of the leading edge excluding the effective zipping zone. C_1, C_2, C_3, and C_4 are fitting parameters, c_i represent magnitudes of forces in the direction of the outward unit normal vector n. The model is solved at each time step in quasi-steady state.

$$\begin{aligned}
\Delta u_i &= 0 \text{ in } D_i \\
u_i &= 0 \text{ on } M^l \cup M^r \\
\frac{\partial u_i}{\partial n} &= C_1 n \text{ on } M^t \cup M^b \\
\frac{\partial u_i}{\partial n} &= C_2 \kappa n + C_3 n \text{ on } \omega_i \backslash Z_i \qquad \text{[Almeida } et\ al \text{ Eq 2]} \\
\frac{\partial u_i}{\partial n} &= C_3 n + \begin{pmatrix} 0 \\ -C_4 \end{pmatrix} \text{ on } \omega_i^t \cap Z_i \\
\frac{\partial u_i}{\partial n} &= C_3 n + \begin{pmatrix} 0 \\ C_4 \end{pmatrix} \text{ on } \omega_i^b \cap Z_i
\end{aligned} \tag{A.9}$$

Table A.5
Parameters for Almeida et al. (2011).

Parameter	Description
C_1	resistance coefficient
C_2	curvature coefficient
C_3	contraction coefficient
C_4	zipping coefficient

Table A.6
Variables for Almeida et al. (2011).

Variable	Description
u_i	displacement field
D_i	position of the epidermis
W_i	position of the amnioserosa
M^l, M^r	left and right boundary of the domain
M^t, M^b	top and bottom boundary of the domain
n	outward unit normal vector to the boundary of D_i
Z_i	effective zipping zone
ω_i	purse string

Appendix A.4. Solon et al., 2009

A viscoelastic vertex model with external forcing applied in parallel to the springs, was used with the purpose of recapitulating cell oscillations during the early stages of dorsal closure. Two types of phenomenological forces are considered with the following magnitudes,

$$F_j = nK\left(1 + \sin\left(\frac{2\pi t}{\omega} + \varphi\right)\right), \quad \text{[Solon } et\ al \text{ Supplemental 1]} \tag{A.10}$$

which includes an explicit time-dependent sine function to generate oscillations.

$$F_j(T) = F_m \frac{T(t-\tau)^h}{T(t-\tau)^h + T_c^h}. \quad \text{[Solon } et\ al \text{ Supplemental 2]} \tag{A.11}$$

This is a Hill function (Hill, 1910) of order h, now applied to force generation. Equation (A.10) was initially used with some success, but failed to recapitulate the antiphase nature of the amnioserosa cell oscillations. Better success in capturing the observed oscillations was achieved using equation (A.11).

Table A.7
Parameters for Solon et al. (2009).

Parameter	Units	Description
$n*K$	dimensionless	amplitude of oscillating force
ω	s	periodicity
φ	dimensionless	phase
h	$\frac{nN}{\mu m * s}$	Hill coefficient: steepness of the force-tension variation
T_c	N	critical cell tension
τ	s	time delay

Table A.8
Variables for Solon et al. (2009).

Variable	Description
F_j	force on each spring of a cell
T	tension of a cell
F_m	maximal contraction force
$T(t-\tau)$	apical AS cell tension at the previous time, $t-\tau$
T_c	critical cell tension

Appendix A.5. Wang et al., 2012

The vertex modeling framework followed in Wang et al. uses a linearized elastic and contractile force in series to describe the force contribution due to the action of actin and myosin (A.12) on cell edges and spokes,

$$f_{i,j} = \mu\left(\ell_{i,j} - \ell_{0i,j}\right) + \beta m_{i,j} \quad \text{[Wang } et\ al \text{ Eq 1]} \tag{A.12}$$

where i and j index nodes and i,j indexes the edge the connects the nodes i and j. The linear elastic term is present on the cell edges and spokes. The second term, providing contractility, is switched on only for the equations describing spoke's forces. For the motion of the cell nodes in the computational model, the fact that the acceleration is negligible in a highly viscous environment with low Reynolds numbers is taken to account in (A.13).

Balance of forces at node i:

$$\eta\frac{d\vec{x_i}}{dt} = \vec{f_i} = \sum_j f_{ij}\frac{\vec{x_j} - \vec{x_i}}{\left|\vec{x_j} - \vec{x_i}\right|} \quad \text{[Wang } et\ al \text{ Eq 2]}. \tag{A.13}$$

The myosin dynamics are described by (A.14)-(A.17), where the signal that activates the myosin production is given by a phenomenological equation (A.16) in absence of any concrete experimental observations and data that could have helped to determine it more precisely.

The kinetic equation for active myosin is modeled by:

$$\frac{dm_{k,j}}{dt} = k^+ s_k h_{kj} - k^- m_{k,j} \quad \text{[Wang } et\ al \text{ Eq 3]}. \tag{A.14}$$

where s_k is the signal level and h_{kj} is a geometric term. The unbinding rate is then treated with an Arrhenius equation:

$$k^- = k_1 e^{-k_2\left[\mu\left(\ell_{k,j} - \ell_{0k,j}\right) + \beta m_{k,j}\right]} \quad \text{[Wang } et\ al \text{ Eq 4]}. \tag{A.15}$$

Myosin dependent rate of change of signaling concentration is tracked by:

$$\frac{ds_k}{dt} = q - k_0 M_k \quad \text{[Wang } et\ al \text{ Eq 5]}. \tag{A.16}$$

$$M_k = \sum_j m_{k,j} \quad \text{[Wang } et\ al \text{ Eq 6]}. \tag{A.17}$$

Table A.9
Parameters for Wang et al. (2012).

Parameter	Units	Description
l_0	μm	rest length of an edge
μ	$\frac{nM}{\mu m}$	elastic modulus of edges
β	$\frac{nN}{\mu M}$	tensile force per myosin motor
η	$\frac{nN*s}{\mu m}$	friction factor

Table A.9 (*continued*)

Parameter	Units	Description
k^+	s^{-1}	myosin association rate: period of oscillations
k^-	s^{-1}	Arrhenius form: load dependent depletion of myosin
q	$\frac{\mu M}{s}$	production rate of signaling
k_0	s^{-1}	signaling depletion coefficient
k_1	s^{-1}	amplitude of cell oscillations
k_2	nN^{-1}	period of cell oscillations (coupled with β)
h_{kj}	dimensionless	geometric factor, which distributes S_k to the different spokes

Table A.10
Variables for Wang et al. (2012).

Variable	Units	Description
$f_{i,j}$	nN	force on the edge connecting nodes i and j
$l_{i,j}$	μm	length of the edge connecting nodes i and j
$m_{i,j}$	μM	myosin concentration in the edge connecting nodes i and j
$\vec{x_i}$	μm	position of node i
f_i	nN	force on node i
$m_{k,j}$	μM	myosin concentration on spoke j in cell k
s_k	nN	signaling concentration in cell k
M_k	nN	myosin concentration in cell k

Appendix A.6. Dierkes et al., 2014

Equation (A.18) is a generic rate equation generalized for dynamic volumes $\left(k_{\text{off}} = \frac{1}{\tau}, k_{\text{on}} = \frac{c}{\tau}\right)$ describing the coupling between the contractile molecule concentration c and the length ℓ of a contractile unit (1D cell). This non-linear model idealizes an amnioserosa cell as a 1-D equivalent circuit. In essence it governs the decay of the total amount of force producing molecules, ℓc, on a cell of length ℓ.

$$\frac{dc}{dt} = -\frac{1}{\tau}(c - c_0) - \frac{c}{l}\frac{dl}{dt} \quad \text{[Dierkes } et\ al \text{ Eq 1]} \tag{A.18}$$

The force balance on a cell is given by the following equation,

$$\mu\frac{dl}{dt} = T_e - T(c) - K(l)\,. \quad \text{[Dierkes } et\ al \text{ Eq 2]} \tag{A.19}$$

A chain of contractile elements is modeled by (A.20) equations where the first two equations described force balance and force generation. The third equation describes an order parameter that tracks synchronous oscillations in a chain of cells.

$$\lambda\frac{dx_n}{dt} = f_n - f_{n-1} \quad f_n = T(c_n) + K(l_n) + \mu\frac{dl_n}{dt}.$$
$$\text{[Dierkes } et\ al \text{ Eq 3]} \tag{A.20}$$

$$\kappa = \max_n \kappa_n, \kappa_n = \left|\int_0^{2\pi} p(\phi)e^{-in\phi}d\phi\right| \quad \text{[Dierkes } et\ al \text{ Eq 4]} \tag{A.21}$$

Table A.11
Parameters for Dierkes et al. (2014).

Variable	Description
c	myosin concentration
l	length of a contractile element
$T(c)$	tension generated by the contractile unit
$K(l)$	elastic restoring force of the spring element
T_e	external tension opposing deformation of the contractile unit
x_n	position of a lattice point
f_n	total force exerted by one contractile unit

Table A.12
Variables for Dierkes et al. (2014).

Parameter	Units	Description
τ	s	turnover time
λ	$\frac{nN*s}{\mu m}$	external friction
μ	$\frac{nN*s}{\mu m}$	damping coefficient
κ	dimensionless	order parameter to quantify clustering

Appendix A.7. Dureau et al., 2016

This model idealizes the tissue as masses and springs, excluding dissipative forces, and tracks the mechanical energy. As discussed in the main text, is not clear how this model can be physically or biologically realistic when applied to dorsal closure. The first three equations are energy equations (see table below) and the fourth equation gives external forces acting on vertices.

$$L_{LEM_i} = \frac{1}{2} m\dot{q}_i(t)^2 - \frac{K_v}{2} \sum_{j \in V(i)} \left(q_i(t) - q_j(t) - l_{1,i,j} \right)^2 - \frac{K_b}{2} \sum_{j \in B(i)} \left(q_i(t) - r_j(t) - l_{2,i,j} \right)^2 \quad \text{[Dureau } et\ al \text{ Eq 1]} \tag{A.22}$$

$$D_{NLVEM_i} = D_{LVEM_i} = \frac{\mu_v}{2} \sum_{j \in V(i)} \left(\dot{q}_i(t) - \dot{q}_j(t) \right)^2 - \frac{\mu_b}{2} \sum_{j \in B(i)} \left(\dot{q}_i(t) - \dot{r}_j(t) \right)^2 \quad \text{[Dureau } et\ al \text{ Page 3]} \tag{A.23}$$

$$L_{NLVEM_i} = L_{LVEM_i} - \frac{k_0}{3} \sum_{j \in B(i)} \left(q_i(t) - r_j(t) - l_{1,i,j} \right)^2 \quad \text{[Dureau } et\ al \text{ Page 3]} \tag{A.24}$$

$$f_i(t) = barA_i \sum_{j \in B(i)} \cos(\omega t + \phi_j), \quad i = 1, 2, \ldots, n_v \quad \text{[Dureau } et\ al \text{ Page 3]} \tag{A.25}$$

The minimization of the defined cost function below

$$\min_{p, q(2), \ldots, q(K)} \sum_{k=2}^{K} \left(y_q(k) - q(k) \right)^2 \quad \text{[Dureau } et\ al \text{ Eq 2a]} \tag{A.26}$$

is constrained by a discretized version of the Euler Lagrange equations below,

$$q(1) - y_q(1) = 0, \quad q(k+1) - F_T(q(k), y_r(k), \dot{y}_r(k), l_0, p) = 0, \quad k = 1, 2, \ldots K-1, \quad \text{[Dureau } et\ al \text{ Eq 2b \& 2c]} \tag{A.27}$$

thus the solution describes mechanical equilibrium or a steady state.

Table A.13
Parameters for Dureau et al. (2016).

Variable	Description
L_{LEM_i}	(linear) total energy of a point mass i
m	point mass
q_i	position of a point mass i
B	barycenter
r_j	position of a cell barycenter
f_i	external forces acting on vertices
D_{LVEM_i}	dissipation of energy due to friction
L_{NLVEM_i}	(non-linear) total energy of a point mass i
D_{NLVEM_i}	(non-linear) dissipation of energy due to friction

Table A.14
Variables for Dureau et al. (2016).

Parameter	Units	Description
K_v	$\frac{kg}{s^2}$	elastic modulus
K_b	$\frac{kg}{s^2}$	elastic modulus
$l_{1,i,j}, l_{2,i,j}$	μm	rest lengths of the springs between vertex i and another vertex or barycenter j
μ_v, μ_b		azimuthal and radial viscosity

References

Almeida, L., Bagnerini, P., Habbal, A., Noselli, S., Serman, F., 2009. Tissue repair modeling. In: Matteo Novaga, G.O. (Ed.), Singularities in Nonlinear Evolution Phenomena and Applications. Edizioni Della Normale, Pisa, Italy, pp. 27–46.

Almeida, L., Bagnerini, P., Habbal, A., Noselli, S., Serman, F., 2011. A mathematical model for dorsal closure. J. Theor. Biol. 268, 105–119.

Anderson, A.R.A., Chaplain, M.A.J., McDougall, S., 2012. A hybrid discrete-continuum model of tumour induced angiogenesis. In: Jackson, T.L. (Ed.), Modeling Tumor Vasculature: Molecular, Cellular, and Tissue Level Aspects and Implications. Springer New York, New York, NY, pp. 105–133.

Begnaud, S., Chen, T., Delacour, D., Mge, R.M., Ladoux, B., 2016. Mechanics of epithelial tissues during gap closure. Curr. Opin. Cell Biol. 42, 52–62. Cell dynamics.

Belacortu, Y., Paricio, N., 2011. Drosophila as a model of wound healing and tissue regeneration in vertebrates. Dev. Dynam. 240, 2379–2404.

Blanchard, G.B., Murugesu, S., Adams, R.J., Martinez-Arias, A., Gorfinkiel, N., 2010. Cytoskeletal dynamics and supracellular organisation of cell shape fluctuations during dorsal closure. Development 137, 2743–2752. http://dev.biologists.org/content/137/16/2743.full.pdf.

Cai, D.J., Aharoni, D., Shuman, T., Shobe, J., Biane, J., Song, W., Wei, B., Veshkini, M., La-Vu, M., Lou, J., Flores, S.E., Kim, I., Sano, Y., Zhou, M., Baumgaertel, K., Lavi, A., Kamata, M., Tuszynski, M., Mayford, M., Golshani, P., Silva, A.J., 2016. A shared neural ensemble links distinct contextual memories encoded close in time. Nature 534, 115 EP –.

Chen, B.C., Legant, W.R., Wang, K., Shao, L., Milkie, D.E., Davidson, M.W., Janetopoulos, C., Wu, X.S., Hammer, J.A., Liu, Z., English, B.P., Mimori-Kiyosue, Y., Romero, D.P., Ritter, A.T., Lippincott-Schwartz, J., Fritz-Laylin, L., Mullins, R.D., Mitchell, D.M., Bembenek, J.N., Reymann, A.C., Böhme, R., Grill, S.W., Wang, J.T., Seydoux, G., Tulu, U.S., Kiehart, D.P., Betzig, E., 2014. Lattice light-sheet microscopy: imaging molecules to embryos at high spatiotemporal resolution. Science 346.

Coravos, J.S., Mason, F.M., Martin, A.C., 2017. Actomyosin pulsing in tissue integrity maintenance during morphogenesis. Trends Cell Biol. 27, 276–283.

Cristini, V., Lowengrub, J., 2010. Multiscale Modeling of Cancer an Integrated Experimental and Mathematical Modeling Approach. Cambridge University Press, Cambridge, UK.

David, D.J.V., Tishkina, A., Harris, T.J.C., 2010. The par complex regulates pulsed

actomyosin contractions during amnioserosa apical constriction in drosophila. Development 137, 1645–1655. http://dev.biologists.org/content/137/10/1645.full.pdf.
Dierkes, K., Sumi, A., Solon, J., Salbreux, G., 2014. Spontaneous oscillations of elastic contractile materials with turnover. Phys. Rev. Lett. 113, 148102.
Ducuing, A., Vincent, S., 2016. The actin cable is dispensable in directing dorsal closure dynamics but neutralizes mechanical stress to prevent scarring in the drosophila embryo. Nat. Cell Biol. 18, 1149 EP –.
Dureau, M., Alessandri, A., Bagnerini, P., Vincent, S., 2016. Modeling and identification of amnioserosa cell mechanical behavior by using mass-spring lattices. IEEE ACM Trans. Comput. Biol. Bioinf. PP, 1–1.
Eltsov, M., Dubé, N., Yu, Z., Pasakarnis, L., Haselmann-Weiss, U., Brunner, D., Frangakis, A.S., 2015. Quantitative analysis of cytoskeletal reorganization during epithelial tissue sealing by large-volume electron tomography. Nat. Cell Biol. 17, 605 EP –.
Fernández, B.G., Arias, A.M., Jacinto, A., 2007. Dpp signalling orchestrates dorsal closure by regulating cell shape changes both in the amnioserosa and in the epidermis. Mech. Dev. 124, 884–897.
Fletcher, A.G., Osborne, J.M., Maini, P.K., Gavaghan, D.J., 2013. Implementing vertex dynamics models of cell populations in biology within a consistent computational framework. Prog. Biophys. Mol. Biol. 113, 299–326.
Franke, J.D., Montague, R.A., Kiehart, D.P., 2005. Nonmuscle myosin ii generates forces that transmit tension and drive contraction in multiple tissues during dorsal closure. Curr. Biol. 15, 2208–2221.
Gates, J., Mahaffey, J.P., Rogers, S.L., Emerson, M., Rogers, E.M., Sottile, S.L., Van Vactor, D., Gertler, F.B., Peifer, M., 2007. Enabled plays key roles in embryonic epithelial morphogenesis in drosophila. Development 134, 2027–2039. http://dev.biologists.org/content/134/11/2027.full.pdf.
Gefen, A. (Ed.), 2013. Multiscale Computer Modeling in Biomechanics and Biomedical Engineering. Springer, Berlin, Heidelberg, Berlin, Heidelberg.
Ghaffarizadeh, A., Heiland, R., Friedman, S.H., Mumenthaler, S.M., Macklin, P., 2018. Physicell: an open source physics-based cell simulator for 3-d multicellular systems. PLoS Comput. Biol. 14, 1–31.
Gorfinkiel, N., 2016. From actomyosin oscillations to tissue-level deformations. Dev. Dynam. 245, 268–275.
Gorfinkiel, N., Blanchard, G.B., 2011. Dynamics of actomyosin contractile activity during epithelial morphogenesis. Curr. Opin. Cell Biol. 23, 531–539. Cell-to-cell contact and extracellular matrix.
Gorfinkiel, N., Blanchard, G.B., Adams, R.J., Martinez Arias, A., 2009. Mechanical control of global cell behaviour during dorsal closure in drosophila. Development 136, 1889–1898. http://dev.biologists.org/content/136/11/1889.full.pdf.
Gorfinkiel, N., Schamberg, S., Blanchard, G.B., 2011. Integrative approaches to morphogenesis: lessons from dorsal closure. Genesis 49, 522–533.
Harden, N., 2002. Signaling pathways directing the movement and fusion of epithelial sheets: lessons from dorsal closure in drosophila. Differentiation 70, 181–203.
Hashimoto, H., Robin, F.B., Sherrard, K.M., Munro, E.M., 2015. Sequential contraction and exchange of apical junctions drives zippering and neural tube closure in a simple chordate. Dev. Cell 32, 241–255.
Hayes, P., Solon, J., 2017. Drosophila dorsal closure: an orchestra of forces to zip shut the embryo. Mech. Dev. 144, 2–10. Roles of physical forces in development.
Heisenberg, C.P., 2009. Dorsal closure in drosophila: cells cannot get out of the tight spot. Bioessays 31, 1284–1287.
Heisenberg, C.P., Bellaïche, Y., 2013. Forces in tissue morphogenesis and patterning. Cell 153, 948–962.
Hill, A.V., 1910. The possible effects of the aggregation of the molecules of hemoglobin on its dissociation curves. J. Physiol. 40 i–vii.
Hill, A.V., 1938. The heat of shortening and the dynamic constants of muscle. Proc. R. Soc. Lond. B Biol. Sci. 126, 136–195. http://rspb.royalsocietypublishing.org/content/126/843/136.full.pdf.
Hunter, G.L., Crawford, J.M., Genkins, J.Z., Kiehart, D.P., 2014. Ion channels contribute to the regulation of cell sheet forces during drosophila dorsal closure. Development 141, 325–334. http://dev.biologists.org/content/141/2/325.full.pdf.
Hutson, M.S., Tokutake, Y., Chang, M.S., Bloor, J.W., Venakides, S., Kiehart, D.P., Edwards, G.S., 2003. Forces for morphogenesis investigated with laser microsurgery and quantitative modeling. Science 300, 145–149.
Jacinto, A., Wood, W., Balayo, T., Turmaine, M., Martinez-Arias, A., Martin, P., 2000. Dynamic actin-based epithelial adhesion and cell matching during drosophila dorsal closure. Curr. Biol. 10, 1420–1426.
Jacinto, A., Wood, W., Woolner, S., Hiley, C., Turner, L., Wilson, C., Martinez-Arias, A., Martin, P., 2002. Dynamic analysis of actin cable function during drosophila dorsal closure. Curr. Biol. 12, 1245–1250.
Jackson, T.L. (Ed.), 2012. Modeling Tumor Vasculature. Springer, New York, NY.
Jankovics, F., Brunner, D., 2006. Transiently reorganized microtubules are essential for zippering during dorsal closure in *Drosophila melanogaster*. Dev. Cell 11, 375–385.
Jayasinghe, A.K., Crews, S.M., Mashburn, D.N., Hutson, M.S., 2013. Apical oscillations in amnioserosa cells: basolateral coupling and mechanical autonomy. Biophys. J. 105, 255–265.
Keener, J., Sneyd, J., 1998. Mathematical Physiology. Springer-Verlag New York, Inc., New York, NY, USA.
Kiehart, D.P., Crawford, J.M., Aristotelous, A.C., Venakides, S., Edwards, G.S., 2017. Cell sheet morphogenesis: dorsal closure in drosophila melanogaster as a model system. Annu. Rev. Cell Dev. Biol. 33, 169–202. PMID: 28992442.
Kiehart, D.P., Galbraith, C.G., Edwards, K.A., Rickoll, W.L., Montague, R.A., 2000. Multiple forces contribute to cell sheet morphogenesis for dorsal closure in drosophila. J. Cell Biol. 149, 471–490. http://jcb.rupress.org/content/149/2/471.full.pdf.
Kong, D., Wolf, F., Grohans, J., 2017. Forces directing germ-band extension in drosophila embryos. Mech. Dev. 144, 11–22. Roles of physical forces in development.
Lacy, M.E., Hutson, M.S., 2016. Amnioserosa development and function in drosophila embryogenesis: critical mechanical roles for an extraembryonic tissue. Dev. Dynam. 245, 558–568.
Layton, A.T., Toyama, Y., Yang, G., Edwards, G.S., Kiehart, D.P., Venakides, S., 2009. Drosophila morphogenesis: tissue force laws and the modeling of dorsal closure. HFSP J. 3, 441–460. PMID: 20514134.
Lo, W.C., Madrak, C., Kiehart, D.P., Edwards, G.S., 2018. Unified biophysical mechanism for cell-shape oscillations and cell ingression. Phys. Rev. E (In review).
Lu, H., Sokolow, A., Kiehart, D.P., Edwards, G.S., 2015. Remodeling tissue interfaces and the thermodynamics of zipping during dorsal closure in *Drosophila*. Biophys. J. 109, 2406–2417.
Lu, H., Sokolow, A., Kiehart, D.P., Edwards, G.S., 2016. Quantifying dorsal closure in three dimensions. Mol. Biol. Cell 27, 3948–3955.
Machado, P.F., Duque, J., Étienne, J., Martinez-Arias, A., Blanchard, G.B., Gorfinkiel, N., 2015. Emergent material properties of developing epithelial tissues. BMC Biol. 13, 98.
Macklin, P., Frieboes, H.B., Sparks, J.L., Ghaffarizadeh, A., Friedman, S.H., Juarez, E.F., Jockheere, E., Mumenthaler, S.M., 2016. Progress towards computational 3-d multicellular systems biology. In: Rejniak (Ed.), Systems Biology of Tumor Microenvironment. Springer chapter 12, pp. 225–246. (invited author: P. Macklin).
Martin, A.C., Goldstein, B., 2014. Apical constriction: themes and variations on a cellular mechanism driving morphogenesis. Development 141, 1987–1998. http://dev.biologists.org/content/141/10/1987.full.pdf.
Martin, P., Wood, W., 2002. Epithelial fusions in the embryo. Curr. Opin. Cell Biol. 14, 569–574.
Millard, T.H., Martin, P., 2008. Dynamic analysis of filopodial interactions during the zippering phase of drosophila dorsal closure. Development 135, 621–626. http://dev.biologists.org/content/135/4/621.full.pdf.
Mortensen, R.D., Moore, R.P., Fogerson, S.M., Chiou, H.Y., Obinero, C.V., Prabhu, N.K., Wei, A.H., Crawford, J.M., Kiehart, D.P., 2018. Identifying genetic players in cell sheet morphogenesis using a drosophila deficiency screen for genes on chromosome 2r involved in dorsal closure. G3: Genes, Genomes, Genetics 8.
Murisic, N., Hakim, V., Kevrekidis, I.G., Shvartsman, S.Y., Audoly, B., 2015. From discrete to continuum models of three-dimensional deformations in epithelial sheets. Biophys. J. 109, 154–163.
Pasakarnis, L., Frei, E., Caussinus, E., Affolter, M., Brunner, D., 2016. Amnioserosa cell constriction but not epidermal actin cable tension autonomously drives dorsal closure. Nat. Cell Biol. 18, 1161. EP –.
Peralta, X.G., Toyama, Y., Hutson, M.S., Montague, R., Venakides, S., Kiehart, D.P., Edwards, G.S., 2007. Upregulation of forces and morphogenic asymmetries in dorsal closure during drosophila development. Biophys. J. 92, 2583–2596.
Peralta, X.G., Toyama, Y., Kiehart, D.P., Edwards, G.S., 2008. Emergent properties during dorsal closure in drosophila morphogenesis. Phys. Biol. 5, 015004–015004.
Pocha, S.M., Montell, D.J., 2014. Cellular and molecular mechanisms of single and collective cell migrations in drosophila: themes and variations. Annu. Rev. Genet. 48, 295–318. PMID: 25421599.
Ray, H.J., Niswander, L., 2012. Mechanisms of tissue fusion during development. Development 139, 1701–1711. http://dev.biologists.org/content/139/10/1701.full.pdf.
Razzell, W., Wood, W., Martin, P., 2014. Recapitulation of morphogenetic cell shape changes enables wound re-epithelialisation. Development 141, 1814–1820.
Rejniak, K.A. (Ed.), 2016. Systems Biology of Tumor Microenvironment. Springer International Publishing, Switzerland.
Saias, L., Swoger, J., D'Angelo, A., Hayes, P., Colombelli, J., Sharpe, J., Salbreux, G., Solon, J., 2015. Decrease in cell volume generates contractile forces driving dorsal closure. Dev. Cell 33, 611–621.
Sharpe, J., 2017. Computer modeling in developmental biology: growing today, essential tomorrow. Development 144, 4214–4225.
Sokolow, A., Toyama, Y., Kiehart, D.P., Edwards, G.S., 2012. Cell ingression and apical shape oscillations during dorsal closure in drosophila. Biophys. J. 102, 969–979.
Solon, J., Kaya-Çopur, A., Colombelli, J., Brunner, D., 2009. Pulsed forces timed by a ratchet-like mechanism drive directed tissue movement during dorsal closure. Cell 137, 1331–1342.
Wada, A., Kato, K., Uwo, M.F., Yonemura, S., Hayashi, S., 2007. Specialized extraembryonic cells connect embryonic and extraembryonic epidermis in response to dpp during dorsal closure in drosophila. Dev. Biol. 301, 340–349.
Wang, Q., Feng, J.J., Pismen, L.M., 2012. A cell-level biomechanical model of drosophila dorsal closure. Biophys. J. 103, 2265–2274.
Wells, A.R., Zou, R.S., Tulu, U.S., Sokolow, A.C., Crawford, J.M., Edwards, G.S., Kiehart, D.P., 2014. Complete canthi removal reveals that forces from the amnioserosa alone are sufficient to drive dorsal closure in drosophila. Mol. Biol.

Cell 25, 3552–3568. http://www.molbiolcell.org/content/25/22/3552.full.pdf+html.
Young, P.E., Richman, A.M., Ketchum, A.S., Kiehart, D.P., 1993. Morphogenesis in drosophila requires nonmuscle myosin heavy chain function. Genes Dev. 7, 29–41.
Yu, J.C., Fernandez-Gonzalez, R., 2017. Quantitative modelling of epithelial morphogenesis: integrating cell mechanics and molecular dynamics. Semin. Cell Dev. Biol. 67, 153–160. Extracellular Vesicles Cellular Mechanisms of Morphogenesis.